C. T. Jolink

Structure-soil interaction for horizontally polarised shear waves

Formulating SH-waves in a homogeneous elastic continuum with generalised boundary conditions

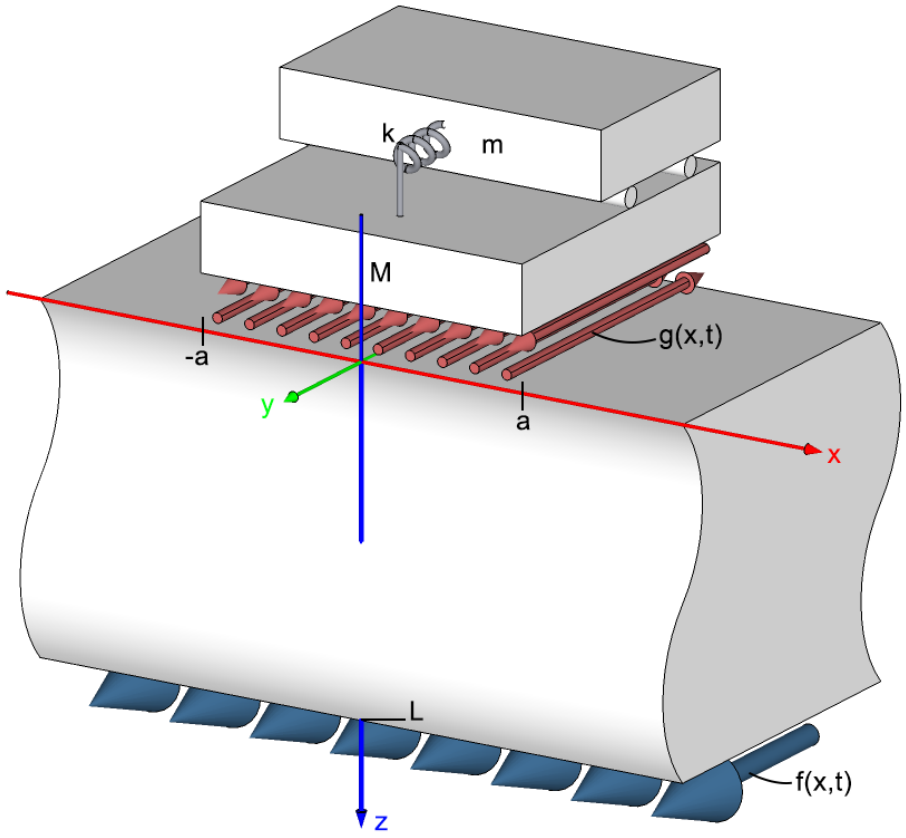

TU Delft

Structure-soil interaction for horizontally polarised shear waves

Formulating SH-waves in a homogeneous elastic continuum with generalised boundary conditions

By

C. T. Jolink

in partial fulfilment of the requirements for the degree of

Master of Science
in Civil Engineering

at the Delft University of Technology,
to be defended on Wednesday November 22, 2017 at 1:00 PM.

Thesis committee:	Dr. ir. K.N. Van Dalen,	TU Delft
	Dr. ir. A. Tsouvalas,	TU Delft
	Ir. M. Zhao,	TU Delft

TU Delft

Preface

This report finalises my study on ‘Structure-soil interaction for horizontally polarised shear waves’ as a minor thesis, in partial fulfilment of my M.Sc.-graduation at the faculty of Civil Engineering and Geosciences of Delft University of Technology. This study is supervised by the section of Structural Mechanics. This study focuses on formulating the dynamic behaviour of an elastic continuum in a general way, that can be applied to various boundary conditions.

My interest for dynamical problems in structural engineering was sparked by Prof. dr. ir. Andrei Metrikine, whose excellent course on *Structural Dynamics* I followed as a part of the curriculum. I found a special appreciation for the beauty of wave phenomena that explain seemingly complicated behaviour so well. I want to thank Prof. dr. ir. Andrei Metrikine for teaching and inspiring me to follow this path in the world of dynamics.

During this study, I found it very satisfying to reach a much better and more fundamental understanding of the dynamic behaviour in structural mechanics. I learned to understand the underlying theory of concepts that I found very abstract before I started this study and I feel much more confident in applying them since. I also learned to see and appreciate the physical meaning of mathematical proceedings. Furthermore, this study gave me the opportunity to discover and learn about the field of Complex Analysis, which I found to be a very powerful tool in evaluating complex integrals. I am sure that this knowledge will be very useful in the future.

I want to thank Dr. ir. Karel van Dalen for explaining abstract concepts so clearly in the course on *Soil Dynamics* and for assigning this minor thesis to me. Most of all, I want to thank my daily supervisor, Ir. Mingjuan Zhao, for her time and effort to answer all my questions and to convince me to keep looking for answers where there didn’t seem to be any.

Lastly, I want to express my gratitude to my parents, who I am greatly indebted to for their unconditional support and trust.

C. T. Jolink
Delft, November 2017

Contents

Abstract

When modelling a structure-soil system, interaction stresses at the interface of the structure and the surface of soil layer influence the dynamic behaviour of the system. These interaction stresses are not accounted for in many simplified models that evaluate the behaviour of the soil layer and the structure separately. Modelling a fully coupled system requires extensive computation that changes with every alteration to the model. Having a general framework of equations that can be easily adapted to each specific case can therefor be of great value.

In this thesis, we model the soil layer as a homogeneous, elastic continuum with two boundary conditions. One boundary condition is a kinematic excitation at the bottom of the soil layer, which is formulated in terms of a Fourier series with prescribed coefficients. The boundary condition at the top of the soil layer is a stress function, formulated as a Fourier series with unknown coefficients. The general solution of the equation of motion is then solved in terms of these known and unknown coefficients. The structure is modelled as an inextensible mass or as a mass-spring system, which is excited by an external force at the interface with the soil layer, formulated in the same Fourier terms and unknown coefficients as for the soil layer. The unknown coefficients are solved by means of an interface condition between the soil layer and the structure.

This computational method provides an equation of motion for the soil layer that depends on the applied structure model. When the structure model is altered, for example by a mass-spring system instead of a single mass, only the interface condition has to be reevaluated to find a solution for the equation of motion of the soil layer and the structure. This thesis shows that this computational model, where we write the specific solution to the equation of motion in terms of unknown Fourier series coefficients, does indeed work.

By analysing the stress distribution at the interface between the soil layer and the structure for different frequencies, results show that the stress is resonant at the natural frequencies of the system. The stress distribution is nearly uniform for most frequencies, but the stresses increase at the sides of the interface at the natural frequencies. It can also be shown that the interaction stresses increase with the frequency.

When analysing various transfer functions, the influence of the stress interaction between the soil layer and the structure is most visible. Computing a fully coupled system shows that the natural frequencies of the system are affected by the structure on the top of the soil layer. First, the natural frequencies are partially shifted to lower frequencies. Secondly, not all natural frequencies lead to infinite resonance: the transfer functions show an alternating pattern of finite and infinite responses to the excitation at the natural frequencies.

The transfer functions of added mass-spring systems, for example, used to model multi story buildings, also shows the influence of the interaction stress compared to the isolated model of the structure. The coupled system shows again that the natural frequencies are partially shifted and not all natural frequencies lead to infinite resonance.

It can be concluded that the interaction stress in a fully coupled system has a significant impact on the system and should be taken into account when modelling a structure-soil system. The tested computational method is good way to do so.

Symbols

Lower case characters

a	distance to edge of the mass along the *x* coordinate
c	damping coefficient
c_s	wave speed
i, j, k	space coordinates *x*, *y* and *z*
i^2	imaginary unit
f_m, g_n	coefficients of mode *m* and *n*, respectively
$f(.)$	displacement function at boundary in time and space domain
$\tilde{f}(.)$	displacement function at boundary in frequency and space domain
$\tilde{\tilde{f}}(.)$	displacement function at boundary in frequency and wave number domain
$g(.)$	stress function at boundary in time and space domain
$\tilde{g}(.)$	stress function at boundary in frequency and space domain
$\tilde{\tilde{g}}(.)$	stress function at boundary in frequency and wave number domain
k	spring stiffness [Pa]
k_m, k_n	wave number of mode *m* and *n*, respectively
k_s, k_x, k_z	components of wave number in respective direction
m	mass of the top block [kg]
m, n, o, p	integers
t	time [s]
u_i	particle displacement of soil in direction *i* in time and space domain
$\tilde{u}_i$	particle displacement of soil in direction *i* in frequency and space domain
$\tilde{\tilde{u}}_i$	particle displacement of soil in direction *i* in frequency and wave number domain
u_m	displacement of mass *m* in time domain
$\tilde{u}_m$	displacement of mass *m* in frequency domain
u_M	displacement of mass *M* in time domain
$\tilde{u}_M$	displacement of mass *M* in frequency domain
$\ddot{u}_m$	acceleration of mass *m* in time domain
$\ddot{u}_M$	acceleration of mass *M* in time domain
x	space coordinate *x*
y	space coordinate *y*
z	space coordinate *z*

Capitals

C	a closed contour in the complex plane
E	Young's modulus [Pa]
F	Force [N]
G	shear modulus [Pa]
$H(.)$	Heaviside step function
K	bulk modulus [Pa] or flexibility matrix
L	depth of source layer from surface [m]
M	mass of the lower block [kg]
P, Q	specific values for integer *p*

X	return distance of periodic function in the space domain [m]

Lower case Greek symbols

α	pole in complex plane
β	parameter representing infinitely small viscous damping
γ	shear angle
$\delta(\,.\,)$	Dirac-delta function
ε	parameter representing infinitely small viscous damping
ε_{ii}	normal strain component on i-surface in i-direction, with $i = x, y, z$
ε_{ij}	shear strain component on i-surface in j-direction, with $i, j = x, y, z$
θ	angle in complex k_x-plane
ν	Poisson's ration, lateral contraction coefficient
ρ	density of soil [kg/m^3] or magnitude of complex value
σ_{ii}	normal stress component on i-surface in i-direction, with $i = x, y, z$
σ_{ij}	shear stress component on i-surface in j-direction, with $i, j = x, y, z$
ω	circular frequency [rad/s]
ω_n	eigenfrequency of mass-spring system [rad/s]

Greek capitals

Γ	contour around a singularity in the complex plane

Subscripts

$u_{y,j}$	the , j refers to the partial derivation with respect to the space coordinate j

1 Introduction

1.1. General

The world we live in never stands still. Everything from subatomic particles to entire galaxies are always moving. People move and nature around us moves. The structures we build are constantly subjected to forces that vary both in time and in space. These dynamic forces influence the behaviour of a structure significantly and in a way that static analysis can not account for.

One way that structures are dynamically loaded is through moving soil. These loads can be human induced by construction work, piling in particular, which is becoming an ever increasing problem in dense cities where nearby buildings are influenced by the vibrations in the soil.
Human made (underground) transportation systems are also notorious for creating waves in the soil. Many modern transportation systems are designed to reduce transportation time, for example by building railroads underground and increasing the velocity of trains. Modern trains can reach velocities of more than 500 km/h where surface waves in the soil are often limited to velocities well below that, depending on the soil composition. When trains exceed the wave propagation velocity, wave radiation occurs and dynamic stresses become very relevant in engineering mechanics of nearby structures.
Earthquakes are another obvious source for dynamic loads through the soil and have become increasingly relevant in the past few years in Groningen, where human induced earthquakes cause a lot of damage to nearby buildings that were not designed for this type of loading.

Implementing dynamic analysis in structural engineering is essential in many cases and a good understanding of soil dynamics to do so is very important. Fortunately, when modelling soil as an elastic continuum, the dynamic behaviour of soil is well understood and derived in a few governing equations that we will touch upon in this dissertation. However, soil in real life is not just an endless (half)space. For practical application of this theory, we need to look beyond the elastic continuum and take a closer look at the boundaries. For example, we may find buildings or other (structural) objects at the soil surface that need to be accounted for when modelling the soil. One of the questions for this thesis that arises is: how does the interaction with objects on the surface impact the behaviour of waves in the soil?

In this study we consider a homogeneous elastic continuum as depicted in figure (1.1) that is excited by a prescribed dynamic displacement as a function of time and space at the bottom at a depth of L, e.g. by an earthquake in a deeper soil layer. At the surface of the soil layer, we consider three cases: the first case is a free field case, where there are no objects on the soil (figure (2.1)). In the second case, an inextensible mass M of width $2a$, from $-a$ to a, rests on the soil. In the third case, we consider a double mass-spring system resting on the soil, where one mass M of width $2a$ is in direct contact with the soil and the other mass m is connected with a spring to mass M (figure (4.1)). The continuum is considered infinite in horizontal directions.

The challenge we face is to formulate applicable governing equations, i.e. an equation of motion for the soil and appropriate boundary conditions at the top and bottom of the elastic layer in a general way, so that it can be tailored to more specific scenarios.

1.2. Aim and scope

This study aims at providing a general framework for calculations that can be used with various kinematic and natural boundary conditions. This framework can then be used to evaluate different scenarios where excitation area, size and type of the mass and the shape and frequency of the excitation may vary. By choosing a modular approach, various mass systems can be applied to solve the interface condition between the soil and the mass to adopt any particular case. This modular approach means that the soil system and the mass system are first evaluated independently by means of a generalised boundary condition at the interface that can be applied to any mass system. This allows us to use the framework for the soil for multiple cases. The generalised boundary conditions of the soil layer and the mass system are then solved with an interface condition to create a fully coupled system. This method contains four fundamental steps:

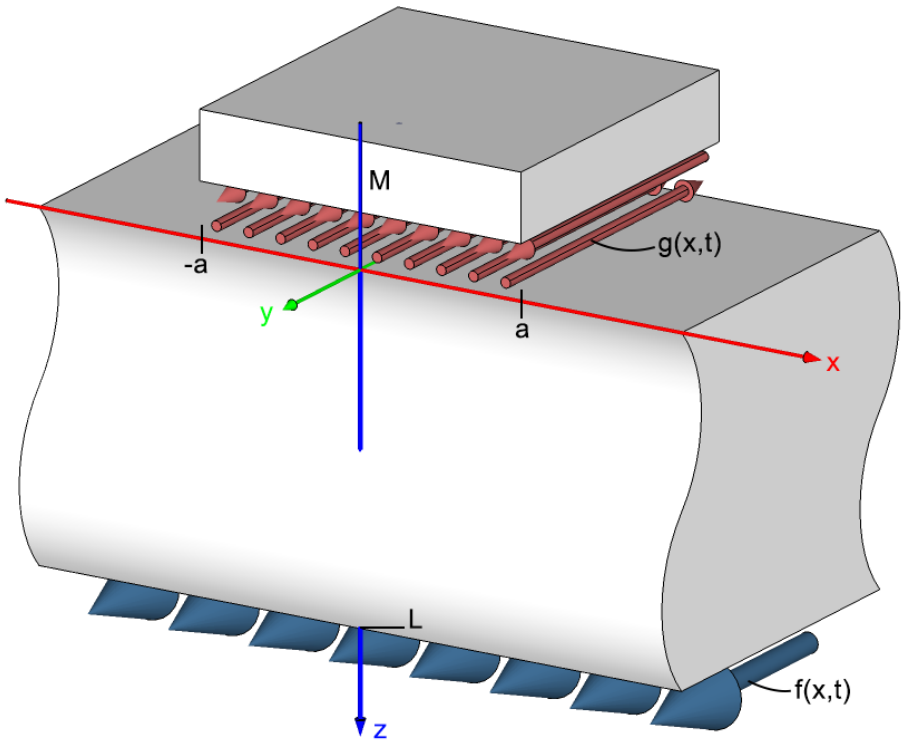

Figure 1.1: a homogeneous elastic soil layer subjected to dynamic, kinematic loading at bottom surface. The red arrows at the top represent the stress function g and the blue arrows at the bottom represent the displacement function f.

- Formulate an equation of motion for the soil layer.
- solve the general solution of the equation of motion in terms of a *known* (kinematic) boundary condition *f* and an *unknown* (stress) boundary condition *g* at the interface.
- Formulate an equation of motion for the mass system with an *unknown* stress boundary condition *g*.
- solve the unknown boundary condition *g* of both systems by means of an interface condition between the systems.

Fourier series will play an important role for this goal, as they allow us to define any shape of the stress distribution *g* between the soil and the mass.

The benefit of this approach is that the mass system can be extended into a multi degree of freedom system without affecting the governing equation of the soil, which makes such an extension far more accessible. You will also have a fully coupled system once the interface condition is solved, so the influence of all parts of the system are taken into account when evaluating the response of any of the parts. The alternative would be to re-evaluate the entire governing equation for the soil for every case or to evaluate responses of isolated systems, which will lead to less accurate results.

The main research question for this thesis is: will this computational method work?

When studying soil dynamics, multiple types of waves can be distinguished and all of these types should be evaluated and combined for a realistic model. These waves include longitudinal waves where particles move in the same direction as the wave propagation, translational waves where the particles move perpendicular to the wave propagation direction and surface waves, which can have various particle motions along the surface of a continuum. Translational waves (or “shear waves”) can be further divided in two categories. Considering the situation as in figure (1.1) from the *x*-*z*-plane, one can distinguish shear waves where:

1. particles move out of plane. This means that for every (in plane) propagation direction of the wave, particles move exclusively horizontally and therefor are appropriately called “horizontally polarised shear waves” or “SH-waves”.
2. particles move in plane. If we consider a horizontal propagation of a wave (i.e. parallel to the *x*-axis), this means that the particles move exclusively vertically (i.e. parallel to the *z*-axis) and therefor are appropriately called “vertically polarised shear waves” or “SV-waves”. Note that when the wave propagates under an angle (but still in plane), particles do not strictly move vertically with respect to the global coordinate system. The particle motion then has to be decomposed in a (coupled) horizontal and vertical motion.

This study solely focusses on SH-waves. In most cases it will be essential to combine the results of this study with those of studies for other wave types, but that will be outside of this study’s scope. We also only focus on steady-state behaviour of the wave.

In this study, we work with a plane situation. An essential assumption that we make is that the gradient out of plane is zero, i.e. that $du/dy = 0$. This implies that the “depth” along the *y*-axis is infinite, which should be considered carefully when using this model for practical application.

The only excitation of the soil that is considered, is by a displacement at the bottom of the soil layer at depth $z = L$. No excitations from the sides or inside the continuum are considered. Because the continuum is infinite in horizontal direction, the radiation boundary condition should be satisfied. The soil is assumed to be homogeneous.

1.3. Outline

In chapter 1 we have so far analysed a problem in the context of soil dynamics and defined the goal of this thesis. We have established a reference frame for the research to come and we have set the scope on assumptions and limitations of the research. The research of this thesis is heavily oriented on finding mathematical expressions for dynamical behaviour where we consider three different cases: free field, single mass and double mass-spring system. These systems are evaluated in chapter 2, 3 and 4, respectively. These chapters are the core of this thesis.

Chapter 2 is entirely devoted to mathematical operations for the free field case and sets a basis for chapter 3 and 4. Chapter 2 is divided in 3 sections that each contain a set of mathematical operations.

Section 2.1 derives the applicable equation of motion of an elastic continuum that is used to model the soil. Starting point is a generalised equation of motion that holds for a homogeneous elastic continuum that will be manipulated for the given case under the assumptions as determined in chapter 1. One important operation that is applied is the Fourier transform to the frequency domain and the wave number domain in order to reduce the equation of motion from a partial differential equation to an ordinary differential equation. A general solution for the equation of motion in the frequency and wave number domain will be the outcome of this section.

Section 2.2 derives the boundary conditions that are needed to solve the general solution from section 2.1. These boundary conditions will be defined by means of Fourier series in order to adapt them to any arbitrary boundary condition that can vary in time and space. One boundary condition (at $z = L$) will be the input function for the dynamical behaviour of the soil and is prescribed through coefficients in the Fourier series. The other boundary condition (at $z = 0$) is defined for the free field case specifically, which means a stress-free surface.

Section 2.3 applies the boundary conditions to the general solution so that the specific solution is expressed in terms of the boundary conditions. After this, the solution (that is still expressed in the wave number domain) is transformed back to the space domain through the inverse Fourier transform. With this solution, the transfer function of the free field soil layer is evaluated.

In chapter 3, we look at the case where a single mass rests on the soil layer. We use the general solution for the equation of motion for the soil from chapter 2.

In section 3.1, we formulate new boundary conditions. We use the same excitation at $z = L$ as in chapter 2 and we formulate a generalised stress function *g* at $z = 0$. The boundary conditions are transformed (with

the Fourier transform) to the frequency- and wave number domain to match the general solution that was derived in chapter 2.

Section 3.2 applies the boundary conditions to the general solution so that the specific solution is expressed in terms of the boundary conditions, i.e. a Fourier series with known coefficients f_m and a Fourier series with unknown coefficients g_n. After this, the solution (that is still expressed in the wave number domain) is transformed back to the space domain through the inverse Fourier transform. This inverse Fourier transform will be done with the method of contour integration and the residue theorem. This section provides the solved equation of motion for the soil with a generalised boundary condition that can be used for any attached multi degree of freedom mass-spring system.

Section 3.3 derives the equation of motion of the single mass system. The boundary condition from section 3.1 at $z = 0$ is used as the external force, which will then also give meaning to this (so far undefined) boundary condition.

Section 3.4 finally solves the interface condition between the soil system and the mass system. Considering that the stress function is a Fourier series with *n* Fourier components, both equations of motion for the soil and the mass are a summation of *n* terms. By applying the orthogonality property, we can derive a flexibility matrix that relates the stress coefficients g_n to the kinematic excitation coefficients f_m. These coefficients can then be solved. Of interest will be the convergence of these coefficients for higher order Fourier components, the convergence of the stress distribution along the interface and the transfer function of the soil and mass.
We compare the transfer function to the one from the free field case to see the influence of the mass on the dynamic behaviour of the soil.

In chapter 4, we look at the case where an additional mass-spring system is attached to the mass resting on the soil layer. We use the specific solution in terms of *f* and *g* for the equation of motion for the soil from chapter 3 again.

In section 4.1, we derive a new equation of motion for the mass-spring system. This will be a set of coupled equations for both masses. The boundary condition from section 3.1 at $z = 0$ is used as the external force. The equations are transformed to the frequency domain to match the interface with the soil.

Section 4.2 will solve the interface condition between the soil system and the mass-spring system, which means that the displacement of the lower mass that is in contact with the soil, must be the same as the displacement of the soil. The orthogonality property is again applied to derive a flexibility matrix that relates the stress coefficients g_n to the kinematic excitation coefficients f_m.
We will look at the convergence of the Fourier components, the stress distribution and the transfer function of the soil again. We compare the transfer function to the free field case and the single mass case to see what influence the added mass spring system has. We will also evaluate the transfer function for the additional mass and compare it to an oversimplified, isolated model. This comparison should tell us how useful it is to consider a fully coupled system (soil and structure) rather than the structure alone.

In chapter 5 we evaluate the results further and conclude our research questions. We finalise the thesis with suggestions for further research.

Appendix A derives the equation of motion of an elastic homogeneous continuum that forms the basis of the equation of motion in chapter 2.

Appendix B explains the concept of contour integration in a complex plane and the application of Cauchy's residue theorem. This theory is used in section 2.3 to evaluate the inverse Fourier transform of the general solution the equation of motion.

2 Free field

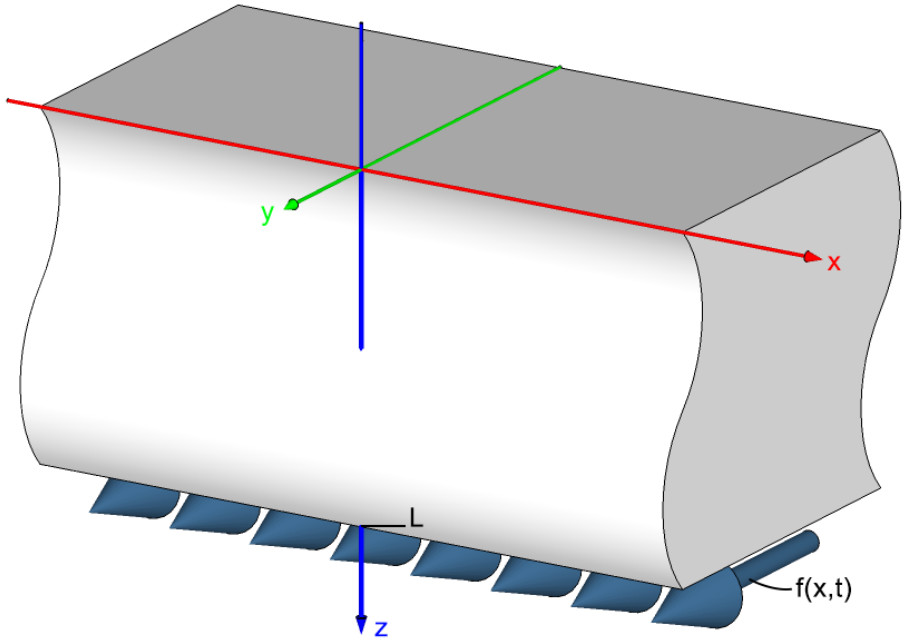

Figure 2.1: a homogeneous elastic soil layer subjected to dynamic, kinematic loading at bottom surface. The top surface is stress free.

To find the response at the surface of the soil to a time dependent displacement in deeper layers of the soil, we need to derive set of governing equations to describe the dynamic behaviour of the soil, modelled as an elastic continuum. The problem description consists of the equation of motion for an elastic continuum and two boundary conditions. One boundary condition describes the motion of the deeper soil layer that acts as the source of the dynamic behaviour and the other boundary condition describes the free traction ($\sigma_{zy} = 0$) at the surface.

2.1. Equation of motion of the elastic continuum

A Cartesian coordinate-system is used in three dimensions. The coordinate system is called the *x-y-z*-system. The displacement is described by three components: u_x, u_y and u_z in *x*, *y*, and *z* direction respectively. The equation of motion of an elastic continuum reads

$$\left(K - \frac{2}{3}G\right) u_{k,ki} + G\left(u_{i,jj} + u_{j,ij}\right) = \rho \ddot{u}_i \tag{2.1}$$

with

K	the bulk modulus [Pa]
G	the shear modulus [Pa]
u_i	the particle displacement in direction *i*
ρ	the density of the continuum [kg/m^3]
i, j, k	space coordinates *x*, *y* and *z*

This equation is derived in appendix A. Note that this equation includes longitudinal waves (also known as “primary waves” or “P-waves”) and transverse waves (also known as “shear waves” or “secondary waves” or “S-waves”).

In a 3D-space, two transverse waves can be distinguished;

- vertically polarised shear waves (“SV-waves”), where particles move along the vertical axis[1], perpendicular to the direction of the wave propagation.
- horizontally polarised shear waves (“SH-waves”), where particles move along a horizontal axis, perpendicular to the direction of the wave propagation.

In this thesis, we will look specifically at SH-waves. To do so, we look at the *x*-*z*-plane under the following assumptions:

$$\begin{cases} \frac{\partial u}{\partial y} = 0 \\ u_x = u_z = 0 \end{cases} \tag{2.2}$$

Under these assumptions, equation (2.1) is only non-trivial for $i = y$, so:

$$\left(K - \frac{2}{3}G\right) u_{k,ky} + G\left(u_{y,jj} + u_{j,yj}\right) = \rho \ddot{u}_y \tag{2.3}$$

Under the same assumptions, this can be reduced to

$$G u_{y,jj} = \rho \ddot{u}_y \tag{2.4}$$

The summation convention applies, which means that identical indices are summed over all space dimensions. This means, explicitly:

$$G\left(u_{y,xx} + u_{y,yy} + u_{y,zz}\right) = \rho \ddot{u}_y \tag{2.5}$$

Again, under the assumption of (2.2), the equation of motion can be further reduced to the final form that is applicable to this particular problem:

$$G\left(u_{y,xx} + u_{y,zz}\right) = \rho \ddot{u}_y \tag{2.6}$$

Or, in a different notation:

$$G\left(\frac{\partial^2}{\partial x^2} + \frac{\partial^2}{\partial z^2}\right) u_y = \rho \frac{\partial^2}{\partial t^2} u_y \tag{2.7}$$

Rewriting equation (2.7) with all constants to the right hand side results in

$$\left(\frac{\partial^2}{\partial x^2} + \frac{\partial^2}{\partial z^2}\right) u_y = \frac{\rho}{G} \frac{\partial^2}{\partial t^2} u_y \tag{2.8}$$

[1] For SV-waves that do not propagate perpendicular to the vertical axis, the particle displacement actually has a vertical and a horizontal component. This situation is beyond the scope of this thesis and therefor not further elaborated.

Equation (2.8) is a partial differential equation with respect to space *x*, space *z* and time *t*. This makes it particularly complicated to find the general solution to the problem. In order to circumvent this complication, we apply the Fourier transform with respect to *t* and *x* to transform the partial differential equation into an ordinary differential equation in the frequency- and wave number domain.

The Fourier transform over time and the inverse Fourier transform over frequency read

$$\tilde{u}_y(x,z,\omega) = \int_{-\infty}^{\infty} u_y(x,z,t) e^{-i\omega t} dt$$
$$u_y(x,z,t) = \frac{1}{2\pi} \int_{-\infty}^{\infty} \tilde{u}_y(x,z,\omega) e^{i\omega t} dt \tag{2.9}$$

with

i	the imaginary unit
t	time
ω	frequency

The physical interpretation of the Fourier transform (2.9) is that we decompose the wave in the time domain into a superposition of waves in the frequency domain.
Applying the Fourier transform (2.9) to the equation of motion (2.8) yields:

$$\left(\frac{\partial^2}{\partial x^2} + \frac{\partial^2}{\partial z^2} \right) \tilde{u}_y = -\omega^2 \frac{\rho}{G} \tilde{u}_y \tag{2.10}$$

Defining the wave speed in the medium as

$$c_s = \sqrt{\frac{G}{\rho}} \tag{2.11}$$

and the squared wave number in the medium as

$$\omega^2 \frac{\rho}{G} = \frac{\omega^2}{c_s^2} = k_s^2 \tag{2.12}$$

we can rewrite (2.10) as

$$\left(\frac{\partial^2}{\partial x^2} + \frac{\partial^2}{\partial z^2} \right) \tilde{u}_y = -k_s^2 \tilde{u}_y \tag{2.13}$$

The Fourier transform over space *x* and the inverse Fourier transform over wave number k_x read:

$$\tilde{\tilde{u}}_y(k_x,z,\omega) = \int_{-\infty}^{\infty} \tilde{u}_y(x,z,\omega) e^{ik_x x} dx$$
$$\tilde{u}_y(x,z,\omega) = \frac{1}{2\pi} \int_{-\infty}^{\infty} \tilde{\tilde{u}}_y(k_x,z,\omega) e^{-ik_x x} dk_x \tag{2.14}$$

with

x	space coordinate *x*
k_x	wave number in *x* direction

Analogue to the Fourier transform over time, the physical interpretation of the Fourier transform over space (2.14) is that we decompose the wave in the space domain into a superposition of waves in the wave number domain.

Applying the Fourier transform (2.14) to the equation of motion (2.13) results in an ordinary differential equation:

$$-k_x^2\tilde{\tilde{u}}_y + \frac{\partial^2}{\partial z^2}\tilde{\tilde{u}}_y = -k_s^2\tilde{\tilde{u}}_y \tag{2.15}$$

Note that both k_s and k_x are wave numbers and that k_x is the horizontal component of k_s. We can therefor combine both quantities in terms of the vertical component of the wave number k_z:

$$k_s^2 - k_x^2 = k_z^2 \tag{2.16}$$

This reduces equation (2.15) to

$$\frac{d^2}{dz^2}\tilde{\tilde{u}}_y + k_z^2\tilde{\tilde{u}}_y = 0 \tag{2.17}$$

The general solution to the homogeneous equation (2.17) reads

$$\tilde{\tilde{u}}_y = Ae^{ik_z z} + Be^{-ik_z z} \tag{2.18}$$

2.2. Boundary conditions

In order to solve the two unknown quantities (A and B) in the general solution (2.18), we need two boundary conditions. Because this is a free field scenario, we can define a zero stress condition at $z = 0$. At $z = L$, we define an input displacement function as a Fourier series with predetermined coefficients f_m.

The benefit of using Fourier series as a boundary condition lies in the fact that any function of space and time can be described, providing a framework for many cases. In this thesis we limit our case to a uniform displacement of the excitation, but we will use the Fourier series notation so that it can be easily adapted for other cases.

2.2.1. Boundary condition at $z = 0$

For the free end of the soil layer, we require the shear stress σ_{zy} to be zero. The stress-free boundary condition in frequency- and wave number-domain reads

$$G\frac{d\tilde{\tilde{u}}(k_x, z, \omega)}{dz}\Big|_{z=0} = 0 \tag{2.19}$$

2.2.2. Boundary condition at $z = L$

We define the displacement u_y of the deep layer as

$$f(x,t) = \sum_m f_m(t)e^{-ik_m x} \tag{2.20}$$

with

k_m	wave number of mode *m*
f_m	coefficient of mode *m*

The wave number k_m of mode *m* is defined as

$$k_m = m\frac{\pi}{X} \tag{2.21}$$

with

m $\in \mathbb{Z}$
X the return distance of the function in the space domain

Note that the function for $f(x,t)$ is a periodic function, which means that the shape of the excitation repeats itself at the distance X. If this characteristic is not desired, it can be limited by a “box function”. This will however make equation (2.20) much more complicated, as we will see in Chapter 3. Alternatively, the influence of the periodic characteristic can be reduced by choosing a very large X in k_m and choosing the coefficients f_m wisely, because the limitation of the excitation area can be “hidden” inside f_m. This method keeps equation (2.20) as simple as possible, which will turn out to be useful in section 2.3. The trade-off is that it will require more modes in the Fourier series to achieve a good approximation of the desired function. Increasing the number of modes increases the computational cost significantly. Given that we only consider a uniform excitation, the return distance X is irrelevant.

Because the equation of motion (2.17) is in the frequency- and wavenumber domain, the boundaries need to be transformed to the same domains according to (2.9) and (2.14) to be compatible.

The Fourier transform over time reads

$$\begin{aligned}\tilde{f}(x,\omega) &= \int_{-\infty}^{\infty} f(x,t)e^{-i\omega t}dt \\ &= \sum_m \tilde{f}_m(\omega)e^{-ik_m x}\end{aligned} \tag{2.22}$$

The Fourier transform of (2.22) over space reads

$$\begin{aligned}\tilde{\tilde{f}}(k_x,\omega) &= \int_{-\infty}^{\infty} \tilde{f}(x,\omega)e^{ik_x x}dx \\ &= \int_{-\infty}^{\infty} \sum_m \tilde{f}_m(\omega)e^{-ik_m x}e^{ik_x x}dx \\ &= \int_{-\infty}^{\infty} \sum_m \tilde{f}_m(\omega)e^{i(k_x-k_m)x}dx \\ &= \sum_m \tilde{f}_m(\omega)2\pi\delta(k_x-k_m)\end{aligned} \tag{2.23}$$

with

δ the Dirac delta function

Having transformed the boundary condition to the appropriate domain, it can now be related to the general solution of the equation of motion (2.18). Recalling that (2.23) is a function for the displacement, the relation becomes

$$\tilde{\tilde{u}}_y(k_x,z,\omega)\Big|_{z=L} = \tilde{\tilde{f}}(k_x,\omega) \tag{2.24}$$

2.3. Solving the general solution

With equation (2.19) and (2.24), we have two algebraic equations with two unknown quantities (A and B):

$$Gik_z \left(Ae^{ik_z z} - Be^{-ik_z z}\right)\Big|_{z=0} = 0 \tag{2.25}$$

$$Ae^{ik_z z} + Be^{-ik_z z}\Big|_{z=L} = \sum_m \tilde{f}_m(\omega) 2\pi\delta(k_x - k_m) \tag{2.26}$$

A and B can now be solved in terms of $\tilde{f}_m$:

$$A = \frac{\sum_m \tilde{f}_m(\omega) 2\pi\delta(k_x - k_m)}{e^{ik_z L} + e^{-ik_z L}} \tag{2.27}$$

$$B = \frac{\sum_m \tilde{f}_m(\omega) 2\pi\delta(k_x - k_m)}{e^{ik_z L} + e^{-ik_z L}} \tag{2.28}$$

Substituting (2.27) and (2.28) in (2.18), the specific solution reads

$$\begin{aligned}\tilde{\tilde{u}}_y(k_x, z, \omega) &= \frac{\sum_m \tilde{f}_m(\omega) 2\pi\delta(k_x - k_m)}{e^{ik_z L} + e^{-ik_z L}} e^{ik_z z} + \frac{\sum_m \tilde{f}_m(\omega) 2\pi\delta(k_x - k_m)}{e^{ik_z L} + e^{-ik_z L}} e^{-ik_z z} \\ &= \sum_m \tilde{f}_m(\omega) 2\pi\delta(k_x - k_m) \frac{\cos\left(\sqrt{k_s^2 - k_x^2} z\right)}{\cos\left(\sqrt{k_s^2 - k_x^2} L\right)}\end{aligned} \tag{2.29}$$

With equation (2.29), we have solved the equation of motion for the free field case in the wave number and frequency domain. The final step is to transform equation (2.29) back to the space x domain by using the inverse Fourier transform (2.14). This gives us:

$$\tilde{u}_y(x, z, \omega) = \sum_m \tilde{f}_m(\omega) \frac{\cos\left(\sqrt{k_s^2 - k_m^2} z\right)}{\cos\left(\sqrt{k_s^2 - k_m^2} L\right)} e^{-ik_m x} \tag{2.30}$$

We can use equation (2.30) as a reference to see how the dynamic behaviour of the soil changes due to shear stresses from objects on the soil in chapter 3 and chapter 4. To do so, we look at the response of the soil at the surface to the frequency of the excitation (“transfer function”) in figure (2.2).

In figure (2.2) we see a pattern of peaks at regular intervals of frequencies. These peaks occur at the *natural frequencies* of the soil and it is a resonance phenomenon. The response at the natural frequencies is (in theory) infinite because we work with an undamped system. In practice this will of course not be the case, as there will always be some damping in every system. In figure (2.2) we look at the range of 0 to 50 Hz where we see 13 natural frequencies. In theory there are infinitely many natural frequencies, but the response at higher frequencies will damp out quickly and are therefor of less interest than lower frequencies. We will only look at the range of 0 to 50 Hz for that reason.

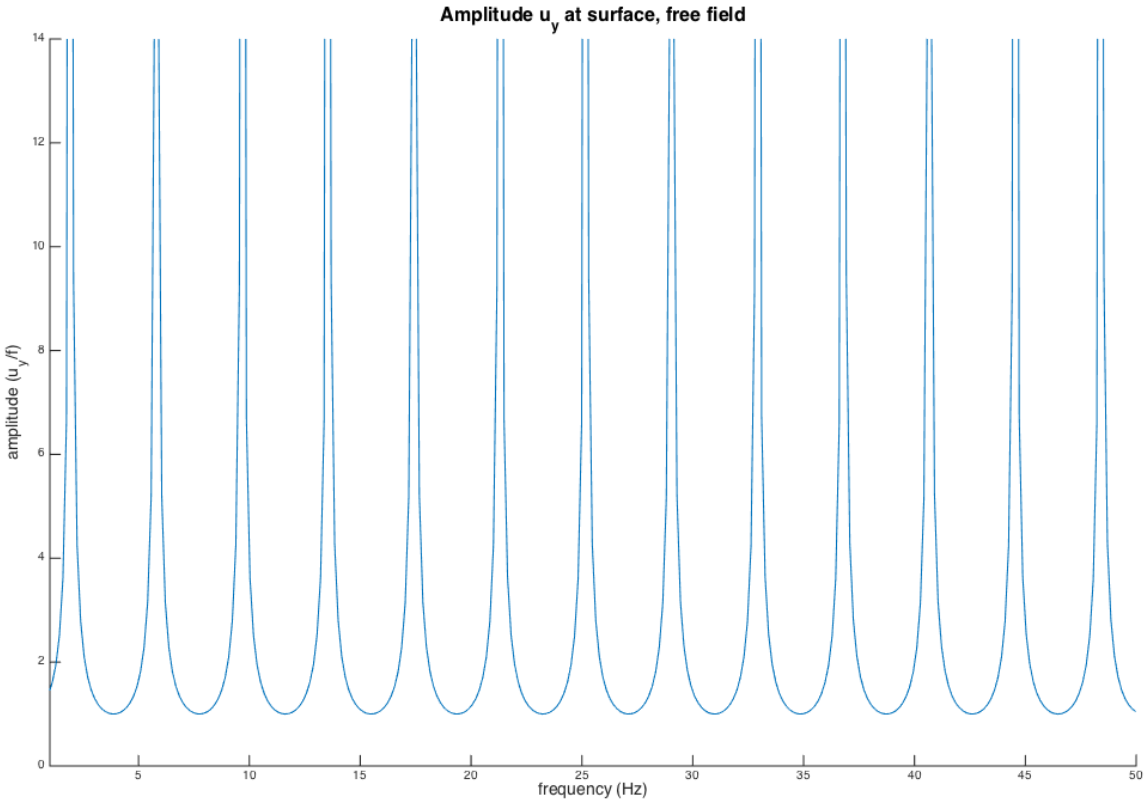

Figure 2.2: transfer function of the free field case.

The reason that resonance occurs at these specific frequencies is that the denominator of equation (2.30) goes to zero. Consider that $k_m = 0$ for the evaluated case, which means that the denominator goes to zero for:

$$\cos\left(\sqrt{k_s^2}L\right) = 0 \rightarrow k_s L = \frac{\pi}{2} + n\pi \tag{2.31}$$

with

$$n \qquad \in \mathbb{Z}$$

Considering that

$$k_s = \frac{\omega}{c_s} \tag{2.32}$$

we find that resonance occurs for

$$\omega = \frac{c_s}{L}\left(\frac{\pi}{2} + n\pi\right) \tag{2.33}$$

This means that we find a resonance peak at the interval of

$$\Delta\omega = \frac{c_s}{L}\pi = \frac{387.3}{50}\pi = 24.3 \text{ rad/s} = 3.8 \text{ Hz} \tag{2.34}$$

We can see that this is consistent with figure (2.2).

3 Single mass

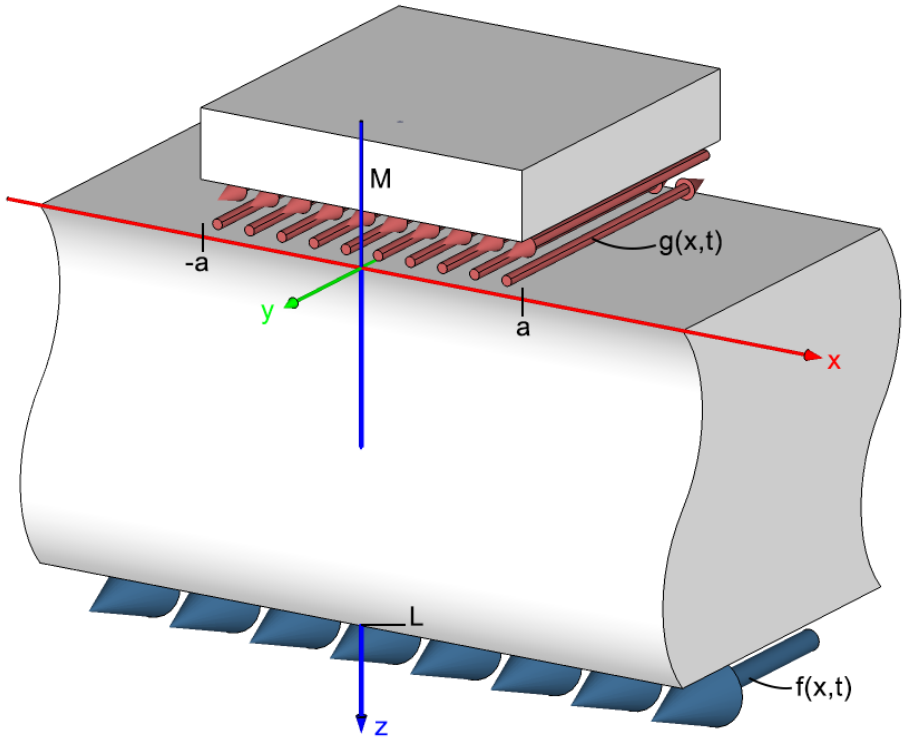

Figure 3.1: a homogeneous elastic soil layer subjected to dynamic, kinematic loading at bottom surface. The red arrows at the top represent the stress function g and the blue arrows at the bottom represent the displacement function f. The structure is modelled as a single, inextensible mass resting on the top of the soil layer.

In this chapter, we will look at the influence that an object resting on the soil has on the response of the soil subject to the excitation at the bottom of the layer. The object consists of a single, inextensible mass *M* of width *2a*, from *-a* to *a*. We assume that the object cannot slip and that its displacement must therefor equal that of the soil (i.e. a continuity interface condition). It will be of particular interest to find the shear stresses σ_{zy} between the soil and the object that we will define as function $g(t,x)$.
This chapter follows up on section 2.1 where we derived the general solution (2.18) for the equation of motion of the soil. Similar to section 2.2 and 2.3, we follow up by defining new boundary conditions for this specific case and solving the general solution (2.18) to obtain a new transfer function. The object on the soil challenges us to use a new approach of computational modelling: we will first define boundary conditions for the dynamic behaviour of the soil in terms of $f(t,x)$ and $g(t,x)$ in section 3.1. We will then formulate an equation of motion for the object that is subject to the stress function $g(t,x)$ in section 3.2. We will finally obtain the unknown coefficients g_n by solving the interface condition between the soil and the object in section 3.3.

3.1. Boundary conditions

In order to solve the two unknown quantities (A and B) in the general solution (2.18), we need two boundary conditions. We define two functions as Fourier series at $z = 0$ and at $z = L$, where one is a response shear stress function with unknown coefficients g_n and one is an input displacement function with predetermined coefficients f_m, like we used for the free field case in chapter 2, respectively.

3.1.1. Boundary condition at $z = 0$

We define the shear stress σ_{zy} as a summation of modes along the applicable length, each as a function of time and space *x*:

$$g(x,t) = \sum_n g_n(t) e^{-ik_n x} \left(H(x+a) - H(x-a) \right) \tag{3.1}$$

with

k_n	wave number of mode *n*
g_n	coefficient of mode *n*
H	Heaviside step function
a	half of the applicable length along the *x* coordinate

The Heaviside step-function H is defined as

$$H(x) = \begin{cases} 1 & \text{if } x > 0 \\ 0 & \text{if } x < 0 \end{cases} \tag{3.2}$$

The wave number k_n of mode *n* is defined as

$$k_n = n \frac{\pi}{X} \tag{3.3}$$

With

n	$\in \mathbb{Z}$
X	the return distance of the function in the space domain.

Given that the function is limited from $-a$ to a due to the Heaviside function, any value for $X \geqslant a$ will do as we are not interested in a repetitive function. In fact, a small value for X (i.e. $X = a$) is preferred because fewer modes are needed to create a detailed function, which can reduce computational cost significantly. We will use $k_n = n\pi/a$ from here on.

Because the equation of motion (2.17) is in the frequency- and wavenumber domain, the boundaries need to be transformed to the same domains according to (2.9) and (2.14) to be compatible. The Fourier transform of (3.1) over time according to (2.9) is straightforward:

$$\begin{aligned} \tilde{g}(x,\omega) &= \int_{-\infty}^{\infty} g(x,t) e^{-i\omega t} dt \\ &= \sum_n \tilde{g}_n(\omega) e^{-ik_n x} \left(H(x+a) - H(x-a) \right) \end{aligned} \tag{3.4}$$

The Fourier transform of (3.4) over space according to (2.14) yields

$$\begin{aligned}\tilde{\tilde{g}}(k_x,\omega) &= \int_{-\infty}^{\infty} \tilde{g}(x,\omega)e^{ik_x x}dx \\ &= \int_{-\infty}^{\infty} \sum_n \tilde{g}_n(\omega)e^{-ik_n x}\left(H(x+a)-H(x-a)\right)e^{ik_x x}dx \\ &= \int_{-a}^{a} \sum_n \tilde{g}_n(\omega)e^{i(k_x-k_n)x}dx \\ &= \sum_n \frac{\tilde{g}_n(\omega)}{i(k_x-k_n)}e^{i(k_x-k_n)x}\Big|_{x=-a}^{x=a} \\ &= \sum_n \tilde{g}_n(\omega)\frac{2\sin\left((k_x-k_n)a\right)}{k_x-k_n}\end{aligned} \tag{3.5}$$

Having transformed the boundary condition to the appropriate domain, it can now be related to the general solution of the equation of motion (2.18). Recalling that (3.5) is a function for the shear stress, the relation becomes

$$G\frac{d\tilde{\tilde{u}}(k_x,z,\omega)}{dz}\Big|_{z=0} = \tilde{\tilde{g}}(k_x,\omega) \tag{3.6}$$

3.1.2. Boundary condition at $z = L$

We use the same boundary condition at $z = L$ as we did in section 2.2.2:

$$f(x,t) = \sum_m f_m(t)e^{-ik_m x} \tag{3.7}$$

We need to transform this boundary condition again to the frequency and wave number domain, where we find from (2.23) that

$$\tilde{\tilde{f}}(k_x,\omega) = \sum_m \tilde{f}_m(\omega)2\pi\delta(k_x-k_m) \tag{3.8}$$

Having transformed the boundary condition to the appropriate domain, it can now be related to the general solution of the equation of motion (2.18). Recalling that (3.8) is a function for the displacement, the relation becomes

$$\tilde{\tilde{u}}_y(k_x,z,\omega)\Big|_{z=L} = \tilde{\tilde{f}}(k_x,\omega) \tag{3.9}$$

3.2. Solving the boundary value problem

With equation (3.6) and (3.9), we have two algebraic equations with two unknown quantities (A and B):

$$Gik_z\left(Ae^{ik_z z}-Be^{-ik_z z}\right)\Big|_{z=0} = \sum_n \tilde{g}_n(\omega)\frac{2\sin\left((k_x-k_n)a\right)}{k_x-k_n} \tag{3.10}$$

$$Ae^{ik_z z}+Be^{-ik_z z}\Big|_{z=L} = \sum_m \tilde{f}_m(\omega)2\pi\delta(k_x-k_m) \tag{3.11}$$

A and B can now be solved in terms of $\tilde{f}_m$ and $\tilde{g}_n$:

$$A = \frac{\left(\sum_m \tilde{f}_m(\omega) 2\pi\delta(k_x - k_m)\right) Gk_z - i\left(\sum_n \tilde{g}_n(\omega) \frac{2\sin\left((k_x - k_n)a\right)}{k_x - k_n}\right) e^{-ik_z L}}{\left(e^{ik_z L} + e^{-ik_z L}\right) Gk_z} \tag{3.12}$$

$$B = \frac{\left(\sum_m \tilde{f}_m(\omega) 2\pi\delta(k_x - k_m)\right) Gk_z + i\left(\sum_n \tilde{g}_n(\omega) \frac{2\sin\left((k_x - k_n)a\right)}{k_x - k_n}\right) e^{ik_z L}}{\left(e^{ik_z L} + e^{-ik_z L}\right) Gk_z} \tag{3.13}$$

Substituting (3.12) and (3.13) in (2.18), the specific solution reads

$$\begin{aligned}\tilde{\tilde{u}}_y(k_x, z, \omega) = &\frac{\left(\sum_m \tilde{f}_m(\omega) 2\pi\delta(k_x - k_m)\right) Gk_z - i\left(\sum_n \tilde{g}_n(\omega) \frac{2\sin\left((k_x - k_n)a\right)}{k_x - k_n}\right) e^{-ik_z L}}{\left(e^{ik_z L} + e^{-ik_z L}\right) Gk_z} e^{ik_z z} \\ &+ \frac{\left(\sum_m \tilde{f}_m(\omega) 2\pi\delta(k_x - k_m)\right) Gk_z + i\left(\sum_n \tilde{g}_n(\omega) \frac{2\sin\left((k_x - k_n)a\right)}{k_x - k_n}\right) e^{ik_z L}}{\left(e^{ik_z L} + e^{-ik_z L}\right) Gk_z} e^{-ik_z z}\end{aligned} \tag{3.14A}$$

This solution can be simplified to

$$\tilde{\tilde{u}}_y(k_x, z, \omega) = \sum_m \tilde{f}_m(\omega)\delta(k_x - k_m)\frac{\cos(k_z z)}{\cos(k_z L)} + \sum_n \tilde{g}_n(\omega)\frac{2\sin\left((k_x - k_n)a\right)}{k_x - k_n}\frac{\sin\left(k_z(z - L)\right)}{\cos(k_z L) Gk_z} \tag{3.14B}$$

From equation (3.14B), we can clearly see that the motion of the soil is a superposition of two distinct waves. The first term relates to the wave caused by the excitation at $z = L$, which behaves as if there were no stress interaction with the mass system ($\tilde{\tilde{\sigma}}_{zy} = 0$). This term is indeed equal to the response from the free field case (equation (2.29)). The second term relates to the wave caused by the stress interaction with the mass system, which behaves as if $\tilde{\tilde{u}}_y = 0$ at $z = L$.

Recall from (2.16) that

$$k_z = \sqrt{k_s^2 - k_x^2} \tag{3.15}$$

In order to solve the interface condition between the displacement of the soil u_y and the displacement of the mass u_M in section 3.4, equation (3.14B) needs to be transformed back to the space x domain through the inverse Fourier transform (2.14):

$$\tilde{u}_y(x, z, \omega) = \frac{1}{2\pi}\int_{-\infty}^{\infty} \tilde{\tilde{u}}_y(k_x, z, \omega) e^{-ik_x x} dk_x \tag{3.16}$$

Evaluating (3.16) can be simplified by splitting (3.14B) into two equations that are evaluated separately and then summed up over. The Fourier transform is a linear operation and therefor the Fourier transform of a summation equals a summation of Fourier transforms:

$$F\left[x(t) + y(t)\right] = F\left[x(t)\right] + F\left[y(t)\right] \tag{3.17}$$

This means that (3.16) can be formulated as

$$\begin{aligned}\tilde{u}_y(x,z,\omega) &= \frac{1}{2\pi}\left(\int_{-\infty}^{\infty}\tilde{\tilde{u}}_{y1}e^{-ik_x x}dk_x + \int_{-\infty}^{\infty}\tilde{\tilde{u}}_{y2}e^{-ik_x x}dk_x\right) \\ &= \tilde{u}_{y1} + \tilde{u}_{y2}\end{aligned} \tag{3.18}$$

with

$$\tilde{u}_{y1}(x,z,\omega) = \frac{1}{2\pi}\sum_m \tilde{f}_m(\omega)\int_{-\infty}^{\infty} 2\pi\delta(k_x - k_m)\frac{\cos\left(\sqrt{k_s^2 - k_x^2}z\right)}{\cos\left(\sqrt{k_s^2 - k_x^2}L\right)}e^{-ik_x x}dk_x \tag{3.19A}$$

$$\tilde{u}_{y2}(x,z,\omega) = \frac{1}{2\pi}\sum_n \tilde{g}_n(\omega)\int_{-\infty}^{\infty}\frac{2\sin\left((k_x - k_n)a\right)}{k_x - k_n}\frac{\sin\left(\sqrt{k_s^2 - k_x^2}(z-L)\right)}{\cos\left(\sqrt{k_s^2 - k_x^2}L\right)G\sqrt{k_s^2 - k_x^2}}e^{-ik_x x}dk_x \tag{3.19B}$$

Evaluating (3.19A) is straightforward as we have already seen in equation (2.30):

$$\tilde{u}_{y1}(x,z,\omega) = \sum_m \tilde{f}_m(\omega)\frac{\cos\left(\sqrt{k_s^2 - k_m^2}z\right)}{\cos\left(\sqrt{k_s^2 - k_m^2}L\right)}e^{-ik_m x} \tag{3.20}$$

Evaluating (3.19B) is far more complex and has to be evaluated using the method of contour integration.

3.2.1. Contour integration

With the method of contour integration in the complex k_x-plane, we can evaluate integral (3.19B) with the help of Cauchy's residue theorem, see Appendix B. To do so, we need to identify all *poles*; a certain type of singularity in a meromorphic function that behaves like the the singularity of $1/z^n$ at $z = 0$.

We find the following simple poles in equation (3.19B):

$$1.\ k_x = k_n = \frac{n\pi}{a}, \quad n \in \mathbb{Z} \tag{3.21A}$$

$$\begin{aligned}2.\ \cos\left(\sqrt{k_s^2 - k_x^2}L\right) = 0 &\Rightarrow \sqrt{k_s^2 - k_x^2}L = \frac{\pi}{2} + p\pi, \quad p \in \mathbb{Z} \\ &\Rightarrow k_x(p) = \pm\sqrt{k_s^2 - \frac{(\frac{\pi}{2} + p\pi)^2}{L^2}}, \quad p \in \mathbb{Z}\end{aligned} \tag{3.21B}$$

All these poles lie on either the real axis or the imaginary axis of the complex k_x-plane, see figure (3.2). The (finite) real-valued poles represent waves traveling to infinity. The (infinite) imaginary-valued poles represent exponentially decaying vibrations ("evanescent waves").
When using the method of contour integration, the signs of k_x and x are very important as they determine the position of the poles in the upper or the lower half of the complex k_x-plane and as a result on which side of the real axis the contour has to be positioned in order to let equation (3.19B) converge. To understand this, we first need to rewrite the first sinus term in (3.19B) in terms of exponential functions.

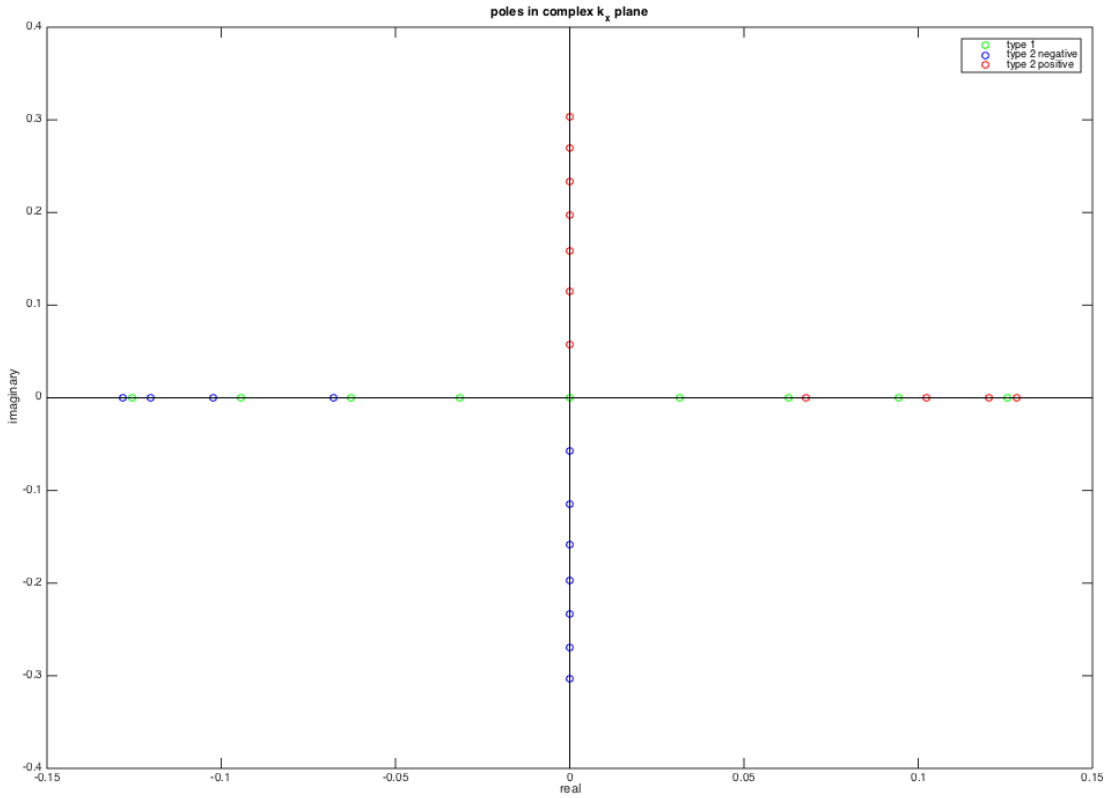

Figure 3.2: Poles in the complex k_x-plane. Number of poles and their positions are indicative!

Considering that

$$2\sin\left((k_x - k_n)a\right) = i\left[e^{-i(k_x-k_n)a} - e^{i(k_x-k_n)a}\right] \tag{3.22}$$

We can then rewrite equation (3.19B) as

$$\tilde{u}_{y2}(x,z,\omega) = \frac{1}{2\pi}\sum_n \tilde{g}_n(\omega)\int_{-\infty}^{\infty}\frac{i}{k_x - k_n}\frac{\sin\left(\sqrt{k_s^2 - k_x^2}(z-L)\right)}{\cos\left(\sqrt{k_s^2 - k_x^2}L\right)G\sqrt{k_s^2 - k_x^2}}\left[e^{-ik_x a}e^{ik_n a} - e^{ik_x a}e^{-ik_n a}\right]e^{-ik_x x}dk_x \tag{3.23}$$

We can now split equation (3.23) in two integrals and focus on the exponentials in these integrals to understand the convergence. Consider that

$$\int_{-\infty}^{\infty}\left[e^{-ik_x a}e^{ik_n a} - e^{ik_x a}e^{-ik_n a}\right]e^{-ik_x x}dk_x = \underbrace{\int_{-\infty}^{\infty}e^{ik_n a}e^{-ik_x(x+a)}dk_x}_{(1)} - \underbrace{\int_{-\infty}^{\infty}e^{-ik_n a}e^{-ik_x(x-a)}dk_x}_{(2)} \tag{3.24}$$

3.2.1.1. First integral

The first integral reads

$$\tilde{u}_{y21}(x,z,\omega) = \frac{1}{2\pi}\sum_n \tilde{g}_n(\omega)\int_{-\infty}^{\infty}\frac{i}{k_x - k_n}\frac{\sin\left(\sqrt{k_s^2 - k_x^2}(z-L)\right)}{\cos\left(\sqrt{k_s^2 - k_x^2}L\right)G\sqrt{k_s^2 - k_x^2}}e^{ik_n a}e^{-ik_x(x+a)}dk_x \tag{3.25}$$

We consider a complex value $k_x = \mathrm{Re}(k_x) + i\mathrm{Im}(k_x)$ and substitute it in (3.25). The convergence of (3.25) will depend on the exponential term:

$$e^{-ik_x(x+a)} = e^{-i\mathrm{Re}(k_x)(x+a)}e^{\mathrm{Im}(k_x)(x+a)} \tag{3.26}$$

For equation (3.26) (and by extend equation (3.25)) to converge, we find the requirement that

$$\mathrm{Im}(k_x)\begin{cases} < 0 & \text{if } x > -a \\ > 0 & \text{if } x < -a \end{cases} \tag{3.27}$$

If we require $x \in [-a, a]$ (which is the contact area between the soil and the mass system), only the first case holds. We can check this by evaluating the integrand of (3.25) as a function of the complex value $k_x = \rho e^{i\theta}$, see figure (3.3).

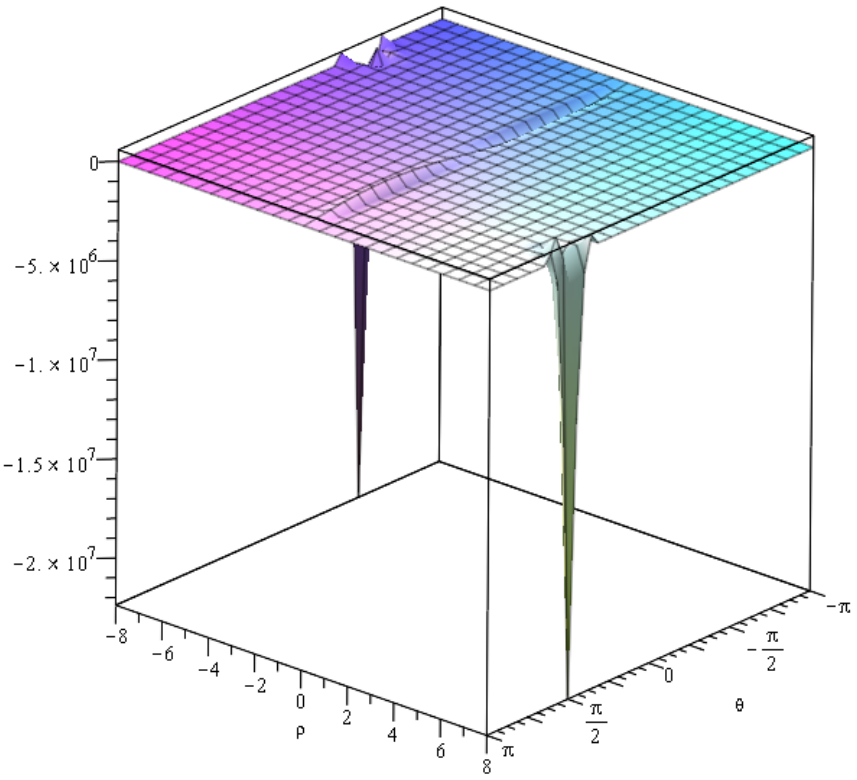

Figure 3.3: integrand of equation (3.25) as a function of k_x.

Figure (3.3) clearly shows that the integrand of (3.25) converges for $\mathrm{Im}(k_x) \to -\infty$ and diverges for $\mathrm{Im}(k_x) \to \infty$. This graph can be interpreted in two ways with the same outcome: with a positive magnitude ($\rho \to \infty$), the function only diverges at $\theta = \pi/2$: the positive part of the imaginary axis. With a negative magnitude ($\rho \to -\infty$), the function diverges at $\theta = -\pi/2$: again at the positive part of the imaginary axis. We can conclude that in order to let (3.25) converge, we should only include poles with a negative imaginary part.

So, when $\mathrm{Im}(k_x) > 0$, the contour has to be placed in the upper half of the complex k_x-plane and when $\mathrm{Im}(k_x) < 0$, the contour has to be placed in the lower half of the complex k_x-plane. From the requirement that $x \in [-a, a]$, it follows that we place the contour of a semi-circle with radius $R \to \infty$ in the lower half of the plane and integrate along the path clockwise, see figure (3.4).

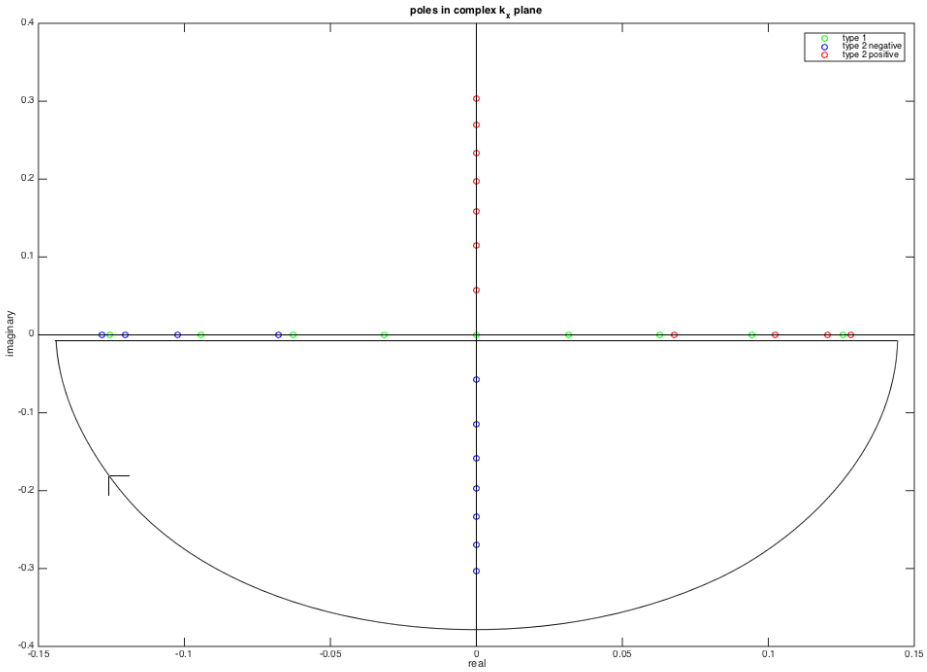

Figure 3.4: Contour for (3.25) of infinite radius. The contour contains infinitely many poles.

3.2.1.2. Second integral
The second integral reads

$$\tilde{u}_{y22}(x,z,\omega) = \frac{1}{2\pi}\sum_n \tilde{g}_n(\omega)\int_{-\infty}^{\infty}\frac{-i}{k_x-k_n}\frac{\sin\left(\sqrt{k_s^2-k_x^2}(z-L)\right)}{\cos\left(\sqrt{k_s^2-k_x^2}L\right)G\sqrt{k_s^2-k_x^2}}e^{-ik_n a}e^{-ik_x(x-a)}dk_x \qquad (3.28)$$

We consider a complex value $k_x = \mathrm{Re}(k_x) + i\mathrm{Im}(k_x)$ again, substitute it in (3.28) and focus on the exponential term:

$$e^{-ik_x(x-a)} = e^{-i\mathrm{Re}(k_x)(x-a)}e^{\mathrm{Im}(k_x)(x-a)} \qquad (3.29)$$

For equation (3.29) to converge, we find the requirement that

$$\mathrm{Im}(k_x)\begin{cases} <0 & \text{if } x>a \\ >0 & \text{if } x<a \end{cases} \qquad (3.30)$$

We require that $x \in [-a,a]$ again and we find that only the second case holds. We can check this again by evaluating (3.28) as a function of the complex value k_x, see figure (3.5). Figure (3.5) clearly shows that the integrand of (3.28) converges for $\mathrm{Im}(k_x) \to \infty$ and diverges for $\mathrm{Im}(k_x) \to -\infty$. We can conclude that in order to let (3.28) converge, we should only include poles with a positive imaginary part.
With these considerations we place the contour of a half circle with radius $R \to \infty$ in the upper half of the plane and integrate along the path anticlockwise, see figure (3.6).

Note that as a consequence of our choice for $x \in [-a,a]$, the solution we find for the displacement field is only valid for the contact area between the soil and the mass system. If we want to compute the displacement at the free surface of the soil, i.e. $x < -a$ or $x > a$, we need to adapt the solution by placing the contours on the opposite sides. This is beyond the scope of this study and will not be evaluated.

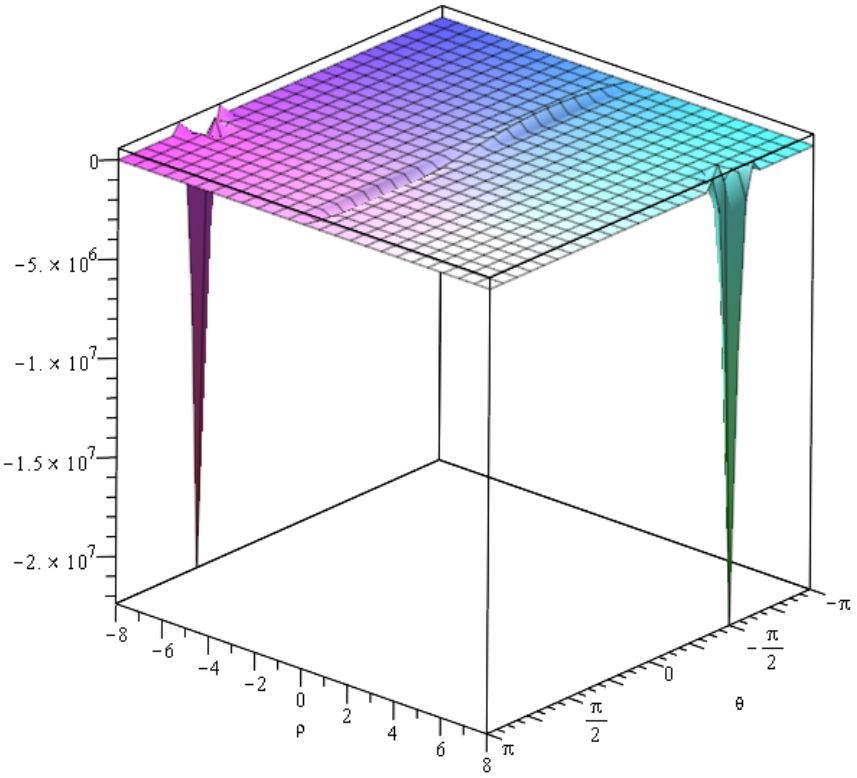

Figure 3.5: integrand of equation (3.28) as a function of k_x.

Poles of type 1 are all real valued and therefor lie on the integration contour and not inside it. Poles of type 2 can be either completely real or completely imaginary and therefor lie partially on and partially inside one of the integration contours. The poles on the integration contour cannot be simply ignored; we need a clever way to determine which poles to include and which poles not.

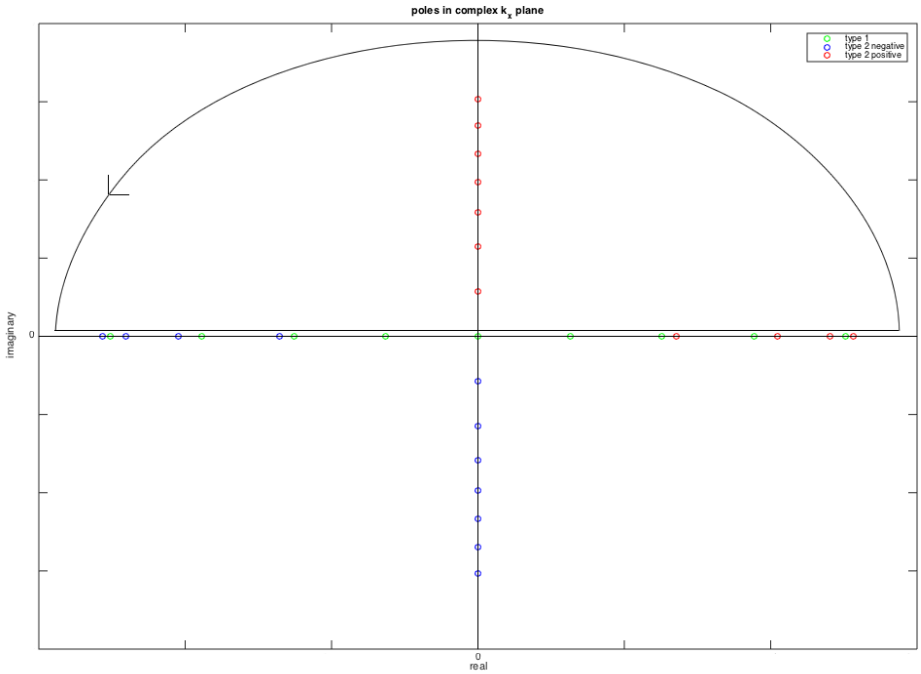

Figure 3.6: Contour for (3.28) of infinite radius. The contour contains infinitely many poles.

3.2.2. Applying viscous damping

The real valued poles of type 2 can be accounted for by adding a small amount of (viscous) damping to the system, which shifts the poles away from the real axis into either the upper or the lower half of the complex plane. This procedure will also shift the poles that lie on the imaginary axis to the side, but this is not relevant for our case and can be ignored. Of particular interest is whether the poles on the real axis move up (away from the contour in the lower half plane and into the contour in the upper half plane) or down (into the contour in the lower half plane and away from the contour in the upper half plane).

In the equation of motion (2.7) we replace the shear stiffness *G* by

$$G \to G\left(1+\beta\frac{d}{dt}\right), \text{ with } \beta = c/G \tag{3.31}$$

with

c damping coefficient

In the frequency domain, the shear stiffness G will be complex and can be written as

$$G \to G\,(1+i\varepsilon), \text{ with } \varepsilon = \frac{\omega c}{G} \ll 1 \tag{3.32}$$

This parameter represents both stiffness and viscous damping, like for an oscillator with parallel spring and damper.

In many cases, a system gives the same result without damping as it will with infinitely small damping (limit case). In this system, this is not the case. Considering that in reality every system has at least a small amount of damping, the limit case will be more realistic than the case without damping and therefor give a more reliable result. This is the reason to add damping to the system to determine the position of the poles.

Recalling the definition of k_s^2 from (2.12), we conclude that the damping makes k_s^2 complex. We therefore change this parameter in (3.21B) to

$$k_s^2 \to \frac{k_s^2}{1+i\varepsilon} \tag{3.33}$$

We use (3.33) to redefine (3.21B) and we expand it into a Taylor series:

$$k_x(p) = \sqrt{\frac{k_s^2}{1+i\varepsilon} - \alpha(p)^2} = \sqrt{k_s^2-\alpha(p)^2}\left(1-\frac{i\varepsilon}{2\left(1-\frac{\alpha(p)^2}{k_s^2}\right)}\right) \tag{3.34}$$

with

$$\alpha(p) = \frac{(\frac{\pi}{2}+p\pi)}{L}, \quad p \in \mathbb{Z} \tag{3.35}$$

The sign of the second term in the brackets in (3.34) determines if the poles on the real axis shift up or down. As we are only interested in the shift of the poles that lie on the real axis, we look at the poles where $\alpha(p) < k_s$. It is apparent that for $\alpha(p) < k_s$ the imaginary part of the complex number $k_x(p)$ is negative. The sign of the second term in the brackets changes for $\alpha(p) > k_s$, but these poles do not lie on the real axis of the complex plane and therefor do not require damping to determine their position. For the negative counterpart of (3.21B), the opposite holds.

Therefor we conclude that;

- The poles of the positive part of (3.21B) that lie on the real axis shift down.
- The poles of the negative part of (3.21B) that lie on the real axis shift up.

Poles of type 1 cannot be shifted by adding viscous damping as they are directly related to the boundaries. These poles are therefor included by expanding the integration contours with small half-circles around the poles and the integration over these poles on the contour is equal to half of the residue. The complex k_x-plane with the poles and the integration contours then looks like figure (3.7).

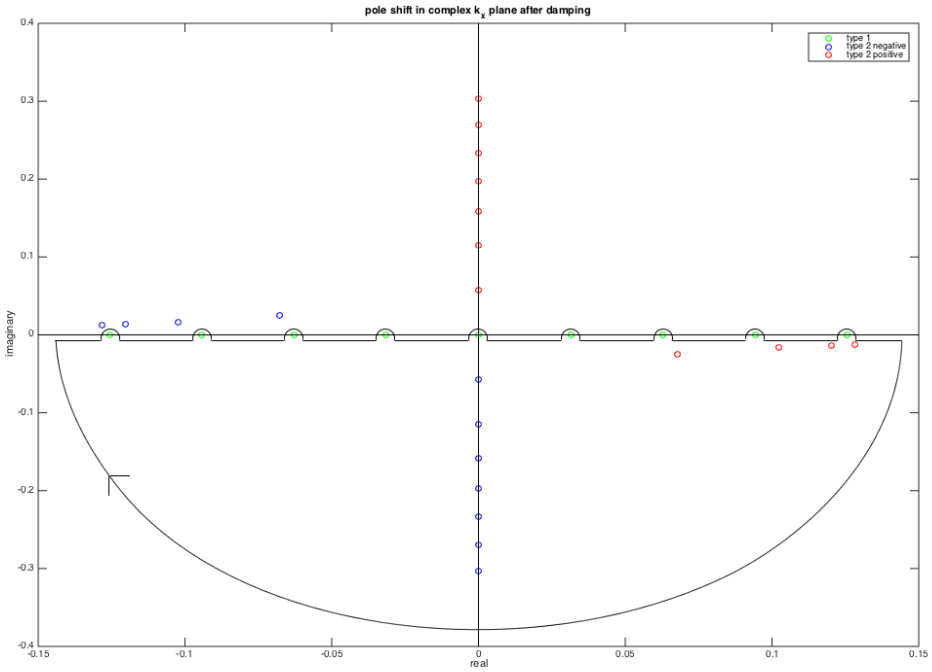

Figure 3.7a: Contour for equation (3.25). The contour now also includes poles on the real axis.

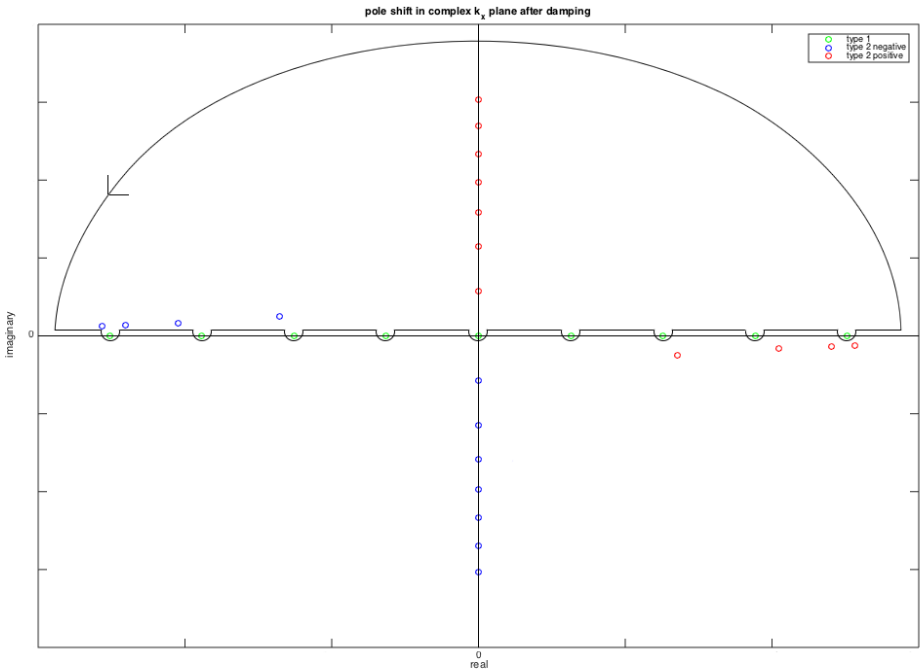

Figure 3.7b: Contour for equation (3.28). The contour now also includes poles on the real axis.

3.2.3. Collecting residues

We can now determine which poles to consider for equation (3.25) and (3.28) and calculate the residues of these poles. With these residues, we can then evaluate the integrals according to the residue theorem and solve equation (3.19B).

3.2.3.1. First integral

We look at equation (3.25) again:

$$\tilde{u}_{y21}(x,z,\omega) = \frac{1}{2\pi}\sum_n \tilde{g}_n(\omega)\int_{-\infty}^{\infty}\frac{i}{k_x-k_n}\frac{\sin\left(\sqrt{k_s^2-k_x^2}(z-L)\right)}{\cos\left(\sqrt{k_s^2-k_x^2}L\right)G\sqrt{k_s^2-k_x^2}}e^{ik_n a}e^{-ik_x(x+a)}dk_x$$

We conclude from figure (3.7a) that the poles that are accounted for are:

$$1.\ k_x = k_n = \frac{n\pi}{a},\quad n\in\mathbb{Z}^2 \tag{3.36A}$$

$$2.\ k_x(p) = \sqrt{k_s^2-\alpha(p)^2},\quad \text{for } \left|\frac{1}{2}+p\right| < \frac{k_s L}{\pi} \tag{3.36B}$$

$$3.\ k_x(p) = -i\sqrt{\alpha(p)^2-k_s^2},\quad \text{for } \left|\frac{1}{2}+p\right| > \frac{k_s L}{\pi} \tag{3.36C}$$

We evaluate (3.25) by finding the residues of these poles. There are infinitely many poles because infinitely many values for *n* and *p* satisfy (3.36A) and (3.36C), respectively. This means that the integral is a summation of infinitely many residues as well and needs to be truncated for practical application. For convenience in writing and to make a clear distinction between real and imaginary poles, let's call all values for *p* that satisfy the condition of (3.36B) *P* and all *p* that satisfy the condition of (3.36C) *Q*.

For (3.25), the residues read:

$$\operatorname*{Res}_{k_x=k_n}(\tilde{u}_{y21}) = \sum_n \tilde{g}_n(\omega)\frac{i\sin\left(\sqrt{k_s^2-k_n^2}(z-L)\right)}{\cos\left(\sqrt{k_s^2-k_n^2}L\right)G\sqrt{k_s^2-k_n^2}}e^{-ik_n x} \tag{3.37A}$$

$$\operatorname*{Res}_{k_x=k_x(P)}(\tilde{u}_{y21}) = \sum_n \tilde{g}_n(\omega)\frac{i\sin\left(|\alpha(P)|(z-L)\right)}{\left(\sqrt{k_s^2-\alpha(P)^2}-k_n\right)GL\sqrt{k_s^2-\alpha(P)^2}\sin\left(|\alpha(P)|L\right)}e^{ik_n a}e^{-i\sqrt{k_s^2-\alpha(P)^2}(x+a)} \tag{3.37B}$$

$$\operatorname*{Res}_{k_x=k_x(Q)}(\tilde{u}_{y21}) = \sum_n \tilde{g}_n(\omega)\frac{-i\sin\left(|\alpha(Q)|(z-L)\right)}{\left(-i\sqrt{\alpha(Q)^2-k_s^2}-k_n\right)GLi\sqrt{\alpha(Q)^2-k_s^2}\sin\left(|\alpha(Q)|L\right)}e^{ik_n a}e^{-\sqrt{\alpha(Q)^2-k_s^2}(x+a)} \tag{3.37C}$$

---

[2] These poles are included in the contour by half a circle around the poles and are therefor only integrated over this half circle. This means that we only consider half of the residues of these poles.

3.2.3.2. Second integral

Now let us look at equation (3.28) again:

$$\tilde{u}_{y22}(x,z,\omega) = \frac{1}{2\pi}\sum_n \tilde{g}_n(\omega)\int_{-\infty}^{\infty}\frac{i}{k_x-k_n}\frac{\sin\left(\sqrt{k_s^2-k_x^2}(z-L)\right)}{\cos\left(\sqrt{k_s^2-k_x^2}L\right)G\sqrt{k_s^2-k_x^2}}e^{-ik_n a}e^{-ik_x(x-a)}dk_x$$

We conclude from figure (3.7b) that the poles that are accounted for are:

$$1.\ k_x = k_n = \frac{n\pi}{a},\quad n\in\mathbb{Z}^3 \tag{3.38A}$$

$$2.\ k_x(p) = -\sqrt{k_s^2-\alpha(p)^2},\quad \text{for } \left|\frac{1}{2}+p\right| < \frac{k_s L}{\pi} \tag{3.38B}$$

$$3.\ k_x(p) = i\sqrt{\alpha(p)^2-k_s^2},\quad \text{for } \left|\frac{1}{2}+p\right| > \frac{k_s L}{\pi} \tag{3.38C}$$

The poles for (3.28) are similar to those of (3.25) except for the signs of type 2 and 3. As for (3.25), there are infinitely many poles because infinitely many values for *n* and *p* satisfy (3.38A) and (3.38C), respectively, which means that the number of poles (and therefor residues) needs to be truncated. In section 3.4.1 will be an example of this truncation. We will make a distinction again for real poles (P) that satisfy the condition of (3.38B) and imaginary poles (Q) that satisfy the condition of (3.38C).

For (3.28), the residues read:

$$\operatorname*{Res}_{k_x=k_n}(\tilde{u}_{y22}) = \sum_n \tilde{g}_n(\omega)\frac{i\sin\left(\sqrt{k_s^2-k_n^2}(z-L)\right)}{\cos\left(\sqrt{k_s^2-k_n^2}L\right)G\sqrt{k_s^2-k_n^2}}e^{-ik_n x} \tag{3.39A}$$

$$\operatorname*{Res}_{k_x=k_x(P)}(\tilde{u}_{y22}) = \sum_n \tilde{g}_n(\omega)\frac{-i\sin\left(|\alpha(P)|(z-L)\right)}{\left(-\sqrt{k_s^2-\alpha(P)^2}-k_n\right)GL\sqrt{k_s^2-\alpha(P)^2}\sin\left(|\alpha(P)|L\right)}e^{-ik_n a}e^{i\sqrt{k_s^2-\alpha(P)^2}(x-a)} \tag{3.39B}$$

$$\operatorname*{Res}_{k_x=k_x(Q)}(\tilde{u}_{y22}) = \sum_n \tilde{g}_n(\omega)\frac{i\sin\left(|\alpha(Q)|(z-L)\right)}{\left(i\sqrt{\alpha(Q)^2-k_s^2}-k_n\right)GLi\sqrt{\alpha(Q)^2-k_s^2}\sin\left(|\alpha(Q)|L\right)}e^{-ik_n a}e^{\sqrt{\alpha(Q)^2-k_s^2}(x-a)} \tag{3.39C}$$

[3] These poles are, again, included in the contour by half a circle around the poles.

3.2.4. Evaluation of the integral

We can now evaluate the integrals according to the residue theorem. For the first integral (3.25), we integrated along the contour clockwise, so it holds that

$$\oint f(z)dz = -2\pi i \sum_n \operatorname*{Res}_{z=z_n}\left(f(z)\right) \tag{3.40A}$$

The second integral (3.28) is integrated along the contour anticlockwise, so it must be evaluated as

$$\oint f(z)dz = 2\pi i \sum_n \operatorname*{Res}_{z=z_n}\left(f(z)\right) \tag{3.40B}$$

Finally, we can conclude from (3.18), (3.24) and (3.40) that

$$\begin{aligned}\tilde{u}_y(x,z,\omega) = \tilde{u}_{y1} &- \frac{2\pi}{2\pi} i \left(\frac{1}{2} \sum_n \operatorname*{Res}_{k_x=k_n} (\tilde{u}_{y21}) + \sum_P \operatorname*{Res}_{k_x=k_x(P)} (\tilde{u}_{y21}) + \sum_Q \operatorname*{Res}_{k_x=-k_x(Q)} (\tilde{u}_{y21}) \right) \\ &- \frac{2\pi}{2\pi} i \left(\frac{1}{2} \sum_n \operatorname*{Res}_{k_x=k_n} (\tilde{u}_{y22}) + \sum_P \operatorname*{Res}_{k_x=-k_x(P)} (\tilde{u}_{y22}) + \sum_Q \operatorname*{Res}_{k_x=k_x(Q)} (\tilde{u}_{y22}) \right)\end{aligned} \tag{3.41}$$

Or, explicitly:

$$\begin{aligned}\tilde{u}_y(x,z,\omega) = &\sum_m \tilde{f}_m(\omega) \frac{\cos\left(\sqrt{k_s^2 - k_m^2}\, z\right)}{\cos\left(\sqrt{k_s^2 - k_m^2}\, L\right)} e^{-ik_m x} \\ &+ \sum_n \tilde{g}_n(\omega) \frac{\sin\left(\sqrt{k_s^2 - k_n^2}(z-L)\right)}{\cos\left(\sqrt{k_s^2 - k_n^2}\, L\right) G\sqrt{k_s^2 - k_n^2}} e^{-ik_n x} \\ &+ \sum_n \sum_P \tilde{g}_n(\omega) \frac{\sin\left(|\alpha(P)|(z-L)\right)}{\left(\sqrt{k_s^2 - \alpha(P)^2} - k_n\right) GL\sqrt{k_s^2 - \alpha(P)^2}\sin\left(|\alpha(P)|L\right)} e^{ik_n a} e^{-i\sqrt{k_s^2 - \alpha(P)^2}(x+a)} \\ &+ \sum_n \sum_Q \tilde{g}_n(\omega) \frac{-\sin\left(|\alpha(Q)|(z-L)\right)}{\left(-i\sqrt{\alpha(Q)^2 - k_s^2} - k_n\right) GLi\sqrt{\alpha(Q)^2 - k_s^2}\sin\left(|\alpha(Q)|L\right)} e^{ik_n a} e^{-\sqrt{\alpha(Q)^2 - k_s^2}(x+a)} \\ &+ \sum_n \sum_P \tilde{g}_n(\omega) \frac{-\sin\left(|\alpha(P)|(z-L)\right)}{\left(-\sqrt{k_s^2 - \alpha(P)^2} - k_n\right) GL\sqrt{k_s^2 - \alpha(P)^2}\sin\left(|\alpha(P)|L\right)} e^{-ik_n a} e^{i\sqrt{k_s^2 - \alpha(P)^2}(x-a)} \\ &+ \sum_n \sum_Q \tilde{g}_n(\omega) \frac{\sin\left(|\alpha(Q)|(z-L)\right)}{\left(i\sqrt{\alpha(Q)^2 - k_s^2} - k_n\right) GLi\sqrt{\alpha(Q)^2 - k_s^2}\sin\left(|\alpha(Q)|L\right)} e^{-ik_n a} e^{\sqrt{\alpha(Q)^2 - k_s^2}(x-a)}\end{aligned} \tag{3.42}$$

3.3. Equation of motion of mass

In this section, we derive the equation of motion for the mass in the time domain and transform it to the frequency domain. We consider an inextensible block that is only constrained by the shear stress at the interface surface with the soil. The equation of motion for the mass reads

$$M\ddot{u}_M = F(t) \tag{3.43}$$

With

M	the mass of the block
u_M	the displacement of the block
F	the external force

Applying the Fourier transform (2.9) to the equation of motion (3.43) yields

$$\tilde{u}_M(\omega) = \int_{-\infty}^{\infty} u_M(t) e^{-i\omega t} dt \tag{3.44}$$

$$-\omega^2 M \tilde{u}_M = F(\omega) \tag{3.45}$$

Considering that the body is inextensible, we only consider rigid body displacements for the mass. We define the external force *F* with the help of (3.4) as

$$\begin{aligned} F(\omega) &= \int_{-a}^{a} \sigma_{zy}(x,\omega) dx \\ &= \int_{-a}^{a} \sum_n \tilde{g}_n(\omega) e^{-ik_n x} dx \\ &= \sum_n \tilde{g}_n(\omega) \frac{-1}{ik_n} e^{-ik_n x} \Big|_{x=-a}^{x=a} \\ &= \sum_n \tilde{g}_n(\omega) \frac{2}{k_n} \sin(k_n a) \end{aligned} \tag{3.46}$$

Combining (3.46) with (3.45) gives the explicit equation of motion for the mass in the frequency domain:

$$\tilde{u}_M = \sum_n \tilde{g}_n(\omega) \frac{-2}{\omega^2 M k_n} \sin(k_n a) \tag{3.47}$$

Considering that $k_n = n\pi/a$, we can immediately see that equation (3.47) will only give a non-trivial result for $n = 0$, because $\lim_{x\to 0} \frac{\sin(x)}{x} = 1$. For every other value of *n,* with *n* being an integer, $\sin(k_n a)$ will be zero. Therefor we find that;

$$\tilde{u}_M = \begin{cases} \tilde{g}_n(\omega) \frac{-2a}{\omega^2 M} & \text{for } n = 0 \\ 0 & \text{for } n \neq 0 \end{cases} \tag{3.48}$$

Equation (3.47) can be used for the interface condition between the soil and the mass at the interface surface. This will ultimately give values to the (so far unknown) coefficients g_n.

3.4. Solving the unknown coefficients

To solve the interface condition at $z = 0$, we combine (3.42) and (3.47) and let $\tilde{u}_y = \tilde{u}_M$. The equation for $\tilde{u}_y$ holds the known excitation modes k_m and coefficients $\tilde{f}_m$ and the unknown stress modes k_n and coefficients $\tilde{g}_n$. The equation for $\tilde{u}_M$ holds the unknown stress modes k_n and coefficients $\tilde{g}_n$. We rearrange the equation such that all unknown terms are on the left hand side and all known excitation terms are on the right hand side:

$$\begin{aligned}
&\sum_n \tilde{g}_n(\omega) \frac{\sin\left(\sqrt{k_s^2 - k_n^2}(-L)\right)}{\cos\left(\sqrt{k_s^2 - k_n^2}L\right) G\sqrt{k_s^2 - k_n^2}} e^{-ik_n x} \\
&+ \sum_n \sum_P \tilde{g}_n(\omega) \frac{\sin\left(|\alpha(P)|(-L)\right)}{\left(\sqrt{k_s^2 - \alpha(P)^2} - k_n\right) GL\sqrt{k_s^2 - \alpha(P)^2}\sin\left(|\alpha(P)|L\right)} e^{ik_n a} e^{-i\sqrt{k_s^2 - \alpha(P)^2}(x+a)} \\
&+ \sum_n \sum_Q \tilde{g}_n(\omega) \frac{-\sin\left(|\alpha(Q)|(-L)\right)}{\left(-i\sqrt{\alpha(Q)^2 - k_s^2} - k_n\right) GLi\sqrt{\alpha(Q)^2 - k_s^2}\sin\left(|\alpha(Q)|L\right)} e^{ik_n a} e^{-\sqrt{\alpha(Q)^2 - k_s^2}(x+a)} \\
&+ \sum_n \sum_P \tilde{g}_n(\omega) \frac{-\sin\left(|\alpha(P)|(-L)\right)}{\left(-\sqrt{k_s^2 - \alpha(P)^2} - k_n\right) GL\sqrt{k_s^2 - \alpha(P)^2}\sin\left(|\alpha(P)|L\right)} e^{-ik_n a} e^{i\sqrt{k_s^2 - \alpha(P)^2}(x-a)} \\
&+ \sum_n \sum_Q \tilde{g}_n(\omega) \frac{\sin\left(|\alpha(Q)|(-L)\right)}{\left(i\sqrt{\alpha(Q)^2 - k_s^2} - k_n\right) GLi\sqrt{\alpha(Q)^2 - k_s^2}\sin\left(|\alpha(Q)|L\right)} e^{-ik_n a} e^{\sqrt{\alpha(Q)^2 - k_s^2}(x-a)} \\
&+ \tilde{g}_0(\omega) \frac{2a}{\omega^2 M} \qquad = \sum_m \tilde{f}_m(\omega) \frac{-1}{\cos\left(\sqrt{k_s^2 - k_m^2}L\right)} e^{-ik_m x}
\end{aligned} \tag{3.49}$$

The final step in solving the governing equation is to decouple the stress modes n as much as possible. We do this by applying the orthogonality property: both sides of the equation are multiplied by $e^{ik_o x}$ and then integrated over *x* from *-a* to *a*, where k_o is defined as

$$k_o = o\frac{\pi}{a} \tag{3.50}$$

with

o $\in \mathbb{Z}$

a the return distance of the function in the space domain.

In short, this means

$$\sum_n \sum_o \tilde{g}_n(\omega) \int_{-a}^{a} (\dots) e^{ik_o x} dx = \sum_m \sum_o \tilde{f}_m(\omega) \int_{-a}^{a} (\dots) e^{ik_o x} dx \tag{3.51}$$

Where the $(\dots)$ represent the terms from equation (3.49).

Given that we work with a coupled system, the system of equations cannot be fully decoupled. This means that we will find a fully populated $n \times n$ flexibility matrix *K* that relates the stress coefficients $\tilde{g}_n$ to the excitation coefficients $\tilde{f}_m$ in the following way:

$$\underbrace{\begin{bmatrix} K_{-N,-N} & \cdots & K_{-N,0} & \cdots & K_{-N,N} \\ \vdots & \ddots & \vdots & \ddots & \vdots \\ K_{0,-N} & \cdots & K_{0,0} & \cdots & K_{0,N} \\ \vdots & \ddots & \vdots & \ddots & \vdots \\ K_{N,-N} & \cdots & K_{N,0} & \cdots & K_{N,N} \end{bmatrix}}_{\substack{K \\ (n\times n)}} \underbrace{\begin{bmatrix} \tilde{g}_{-N} \\ \vdots \\ \tilde{g}_0 \\ \vdots \\ \tilde{g}_N \end{bmatrix}}_{\substack{\tilde{g} \\ (n\times 1)}} = \underbrace{\begin{bmatrix} \tilde{f}_{-N} \\ \vdots \\ \tilde{f}_0 \\ \vdots \\ \tilde{f}_N \end{bmatrix}}_{\substack{\tilde{f} \\ (n\times 1)}} \tag{3.52}$$

Now that we know how to formulate the flexibility matrix and the relation between the excitation and the stress coefficients, we can solve the equation to find the stress coefficients. With these stress coefficients we can use equation (3.42) to compute the response of the soil to the excitation and compare it to the free field case.
So far, we used a generalised and analytical approach in order to define the interaction stresses between the soil layer and the mass. For the next step, a numerical approach is necessary and we need to assume certain values for all parameters. The results from these assumptions are therefor only valid for this specific case and need to be reevaluated when different parameters are used!

Parameters			
ρ	2000 [kg/m^3]	M	25 000 [kg]
a	10 [m]	G	3*10^8 [n/m^2]
L	50 [m]	X	10 [m]

The number of poles *p* and the number of modes *n* are to be chosen such that the stress distribution and the transfer function lead to a converged result, based on the assumed parameters. It is hard to say a priori how many poles and modes need to be considered for a converged result, so we will look at the relation between these numbers in the following sections.

3.4.1. Convergence of poles

As we have discussed in section 3.2.3, there are infinitely many poles that satisfy (3.36C) and (3.38C) and therefor (3.49) contains infinitely many terms. In section 3.2.1 we already made sure that the summation of these terms must converge and we can therefor truncate the number of poles. The truncation influences the entries in the flexibility matrix. Figure (3.8) shows six examples of how the entry $K_{N,N}$ (see equation (3.52)) in the flexibility matrix of the residue of the imaginary poles changes (cumulatively) for each pole, depending on frequency ω and number of modes *n*.

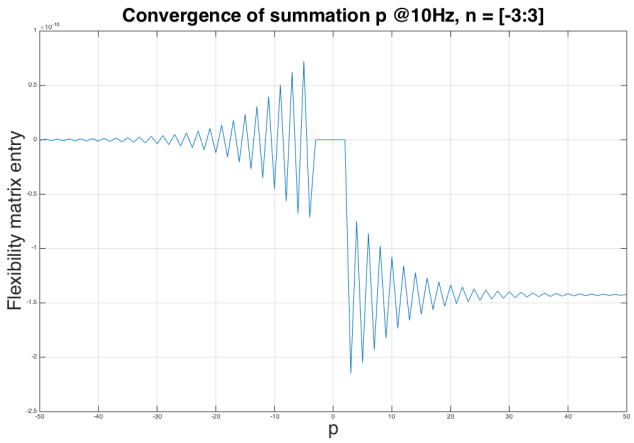

Figure 3.8a: Convergence of p at 10Hz, n=[-3:3]

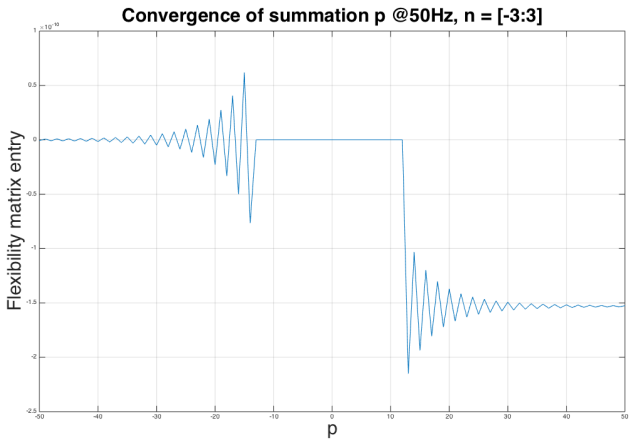

Figure 3.8b: Convergence of p at 50Hz, n=[-3:3]

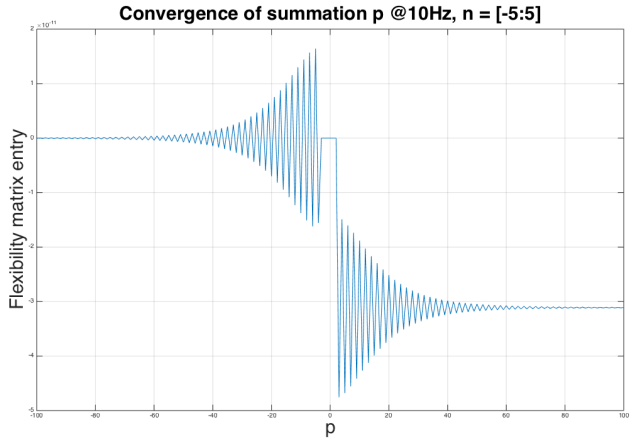

Figure 3.8c: Convergence of p at 10Hz, n=[-5:5]

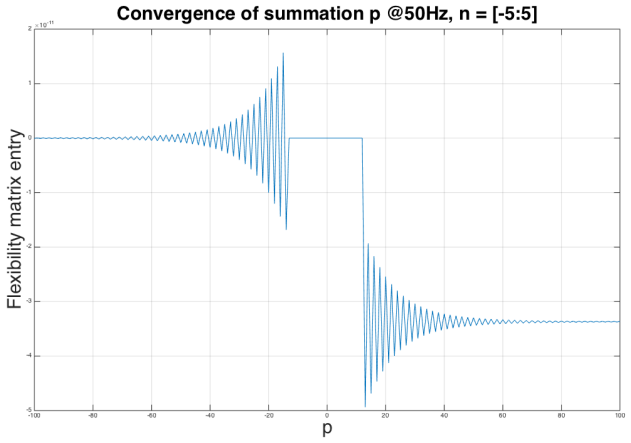

Figure 3.8d: Convergence of p at 50Hz, n=[-5:5]

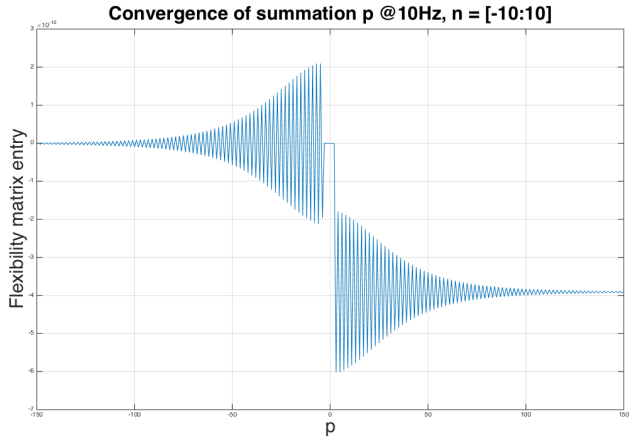

Figure 3.8e: Convergence of p at 10Hz, n=[-10:10]

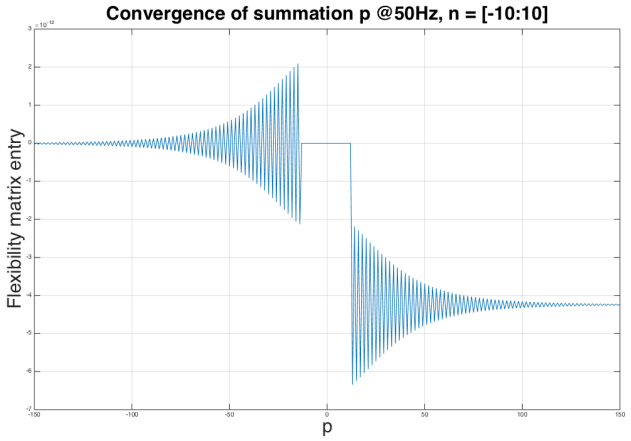

Figure 3.8f: Convergence of p at 50Hz, n=[-10:10]

Figure (3.8) shows a few consistent characteristics: for all frequencies and ranges of modes, the first (most negative) pole adds an insignificant amount to the converged result and hence the entry starts at zero. This makes sense as we are looking for a range of poles with converging attribution for both extremes: positive and negative. The attribution of each pole grows with alternating signs as they get closer to $p = 0$ and ultimately converge to the final result as *p* becomes larger.

The number of poles *p* to reach a converged result increases when the number of modes *n* increases. For the range $n = [3 : 3]$, *p* needs a range of roughly $p = [-50 : 50]$ to converge. For $n = [5 : 5]$, *p* needs a range of roughly $p = [-100 : 100]$. For $n = [10 : 10]$, *p* needs a range of roughly $p = [-150 : 150]$. Using more poles is, of course, always allowed. Using a range of $p = [-200 : 200]$ ensures a properly converged result for even higher ranges of *n*. Computational cost increases significantly when using more poles than necessary, so it is wise to adjust the range of poles to the range of modes in the model.

There is a noticeable gap in the plots around $p = 0$ where no contribution is added. These centre poles represent the real valued poles that are finite and do not add to the residue of imaginary poles. We can see that the gap widens for higher frequencies, from which we can conclude that more traveling waves occur in the system at higher frequencies compared to lower frequencies.

3.4.2. Solving stress coefficients g_n

With equation (3.49) and equation (3.51), we know how to populate the flexibility Matrix *K* of the system. We have also empirically found how many poles *p* need to be included to find a converged result for *K*. With equation (3.52) we can finally solve the stress coefficients g_n:

$$\tilde{g}_n = K^{-1}\tilde{f}_m \tag{3.53}$$

With equation (3.4) and equation (3.53) we can then plot the stress distribution at the interface. Figure (3.9) shows the coefficients $\tilde{g}_n$ and the stress distribution $\tilde{g}(\omega, x)$ for $n = [-3 : 3]$ at 43.8 Hz and 44.7 Hz. Figure (3.10) shows the coefficients and the stress distribution for $n = [-5 : 5]$. Figure (3.11) for $n = [-10 : 10]$.

Figure 3.9a: Coefficients g_n, n=[-3:3]

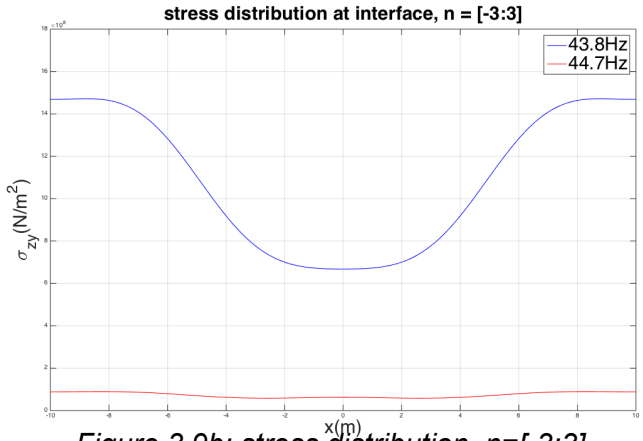

Figure 3.9b: stress distribution, n=[-3:3]

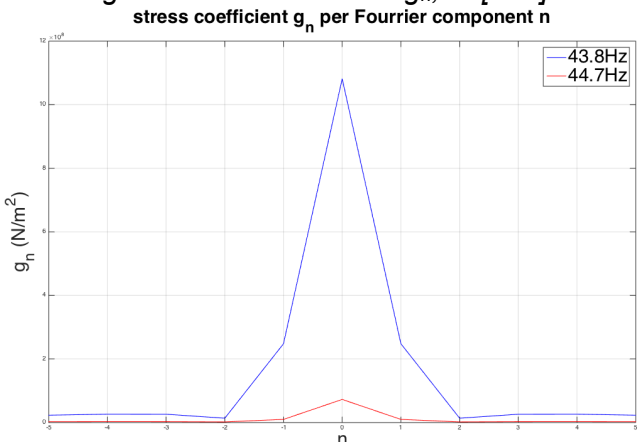

Figure 3.10a: Coefficients g_n, n=[-5:5]

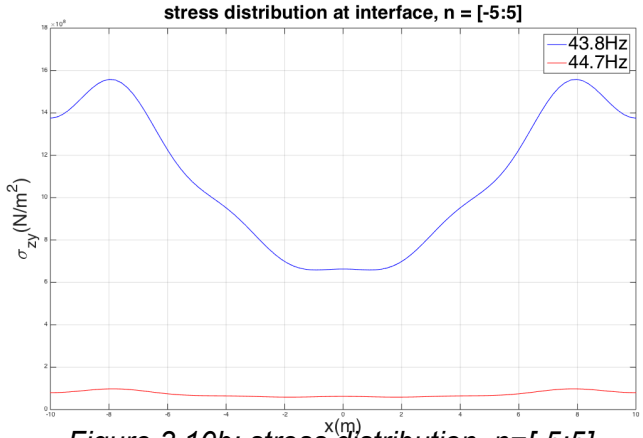

Figure 3.10b: stress distribution, n=[-5:5]

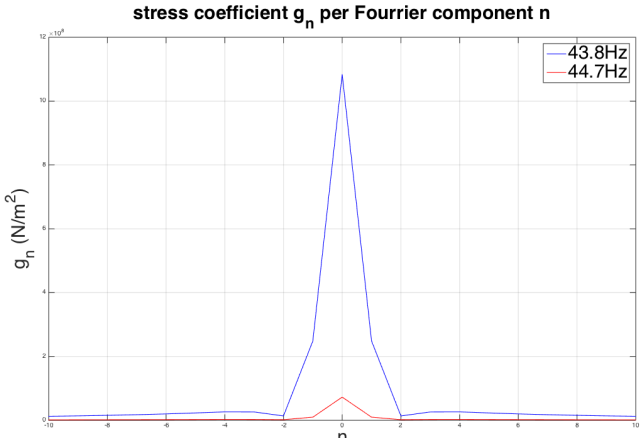

Figure 3.11a: Coefficients g_n, n=[-10:10]

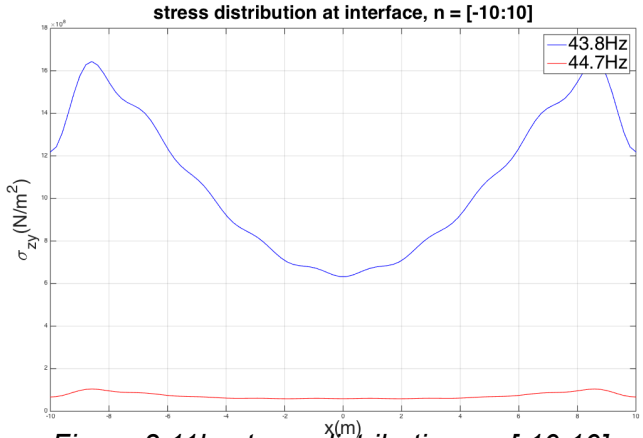

Figure 3.11b: stress distribution, n=[-10:10]

From figure (3.9), (3.10) and (3.11) we can draw a few conclusions:

First of all, the frequency at which the stresses are analysed is of great relevance. As we can see from the figures above, stresses can easily change tenfold by changing the frequency by as little as 0.9 Hz. The chosen frequencies of 43.8 Hz and 44.7 Hz are not arbitrary: 43.8 Hz is one of the many natural frequencies of the system at which resonance occurs. Resonance does not only affect the kinematic amplitude of the response (as we have already seen in figure (2.2)), but also the interface stresses in this coupled model. At 44.7 Hz, the model shows very little response. The stress coefficient for the centre Fourier component, g_0, is plotted against the frequency range in figure (3.12).

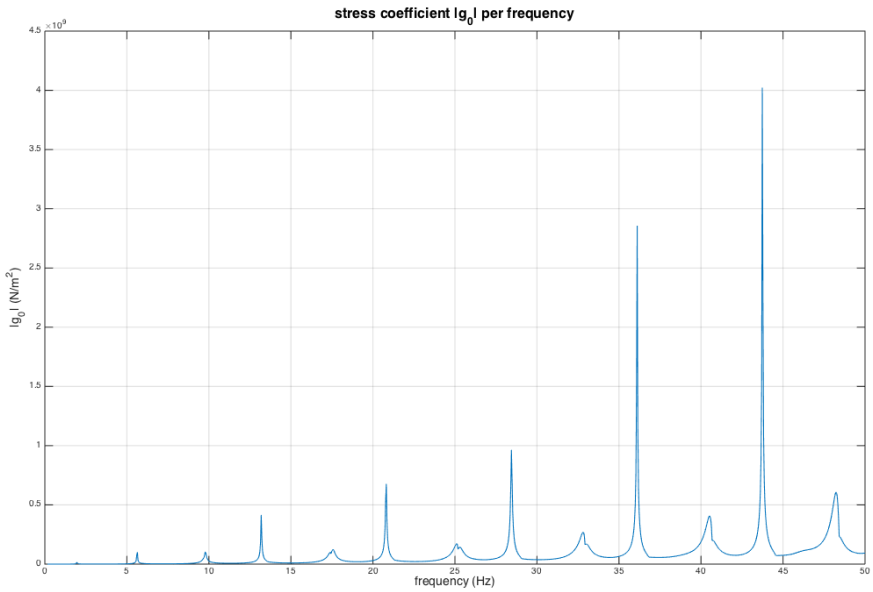

Figure 3.12: coefficient $|g_0|$ per frequency.

Figure (3.12) shows that the average stress is subject to resonance. We will see resonance at the same frequencies in the transfer function in figure (3.15). There appears to be an exponential growth for every natural frequency.

We see for both frequencies and all ranges of *n* that the centre Fourier component, $n = 0$, has by far the largest contribution with a quick drop off and convergence to zero as $|n| \to \infty$. At 44.7 Hz, g_1 and g_{-1} show very little contribution and all other components are nearly zero. The result is a fairly uniform stress distribution that does not change significantly when using more modes. A small range of modes, e.g. $n = [-3 : 3]$ should suffice to compute these low stresses. At 43.8 Hz, g_1 and g_{-1} show a significantly larger contribution and also higher order components contribute to the stress distribution. The stress distribution changes noticeably when using more modes and is far from uniform. At natural frequencies like 43,8 Hz, using a range of at least $n = [-10 : 10]$ is strongly recommended!

In figure (3.13) we directly compare the stress distributions at 43.8 Hz for different number of modes to see how it converges.

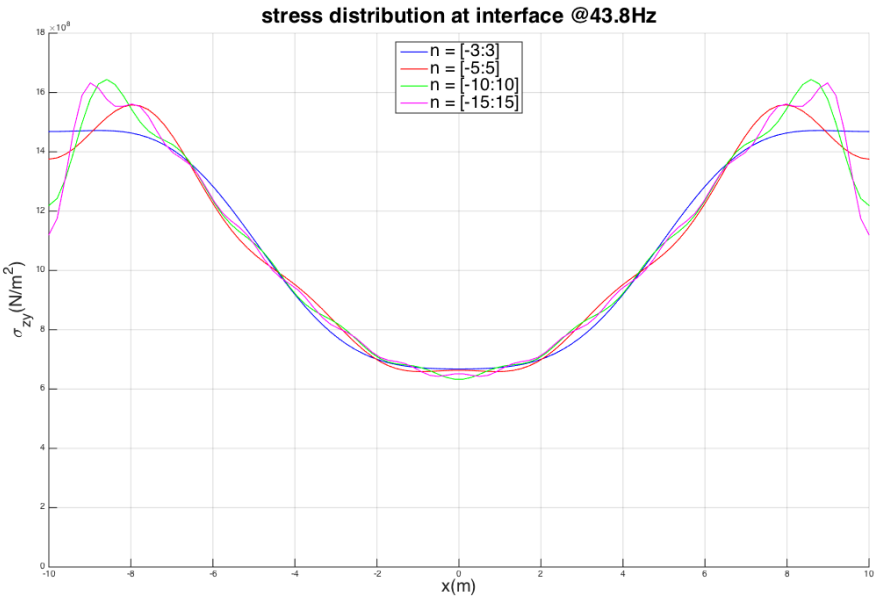

Figure 3.13: stress distribution at interface for different number of modes.

Figure (3.13) shows that the centre part of the stress distribution, roughly in the range of $x = [-6 : 6]$ m, converges quickly and a range for *n* as low as $n = [-3 : 3]$ gives fairly accurate results. At the sides of the interface however, the result has not converged up to $n = [-15 : 15]$ and even more modes are required for accurate results.

3.4.2. Analysing the transfer function

With the stress coefficients g_n known, we can use (3.47) to evaluate the displacement of the mass $\tilde{u}_M$ and we can compare it to the free field case figure (2.2).

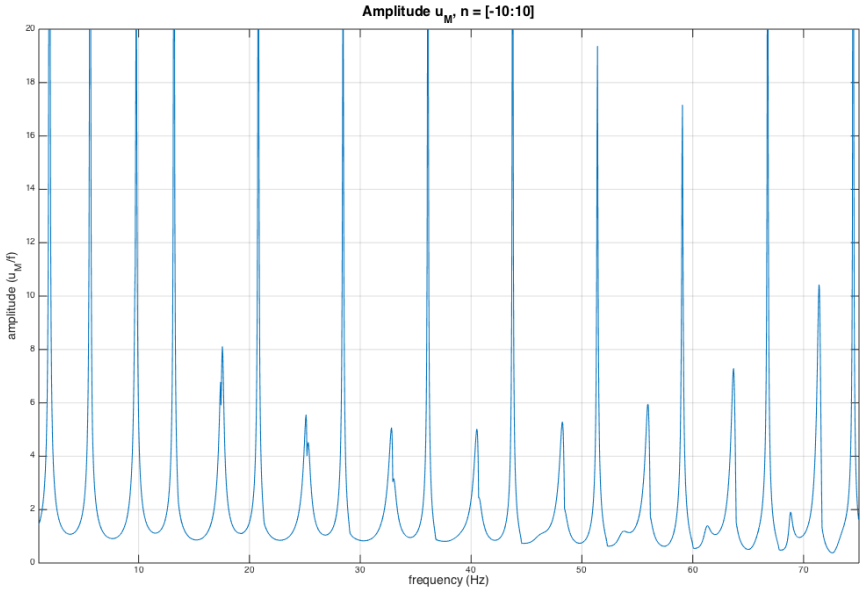

Figure 3.14: transfer function of soil-mass system.

The transfer function in figure (3.14) shows a pattern of peaks similar to the free field case in figure (2.2). These peaks occur at the natural frequencies of the system and are therefor a consequence of resonance. These frequencies are the same as for the stress peaks in figure (3.12). Unlike the free field case, not all peaks are infinitely large: we see an alternating pattern of small and large (infinite) peaks. The reason for this can be found in the first two terms of equation (3.42):

$$\tilde{u}_y(x,z,\omega) = \sum_m \tilde{f}_m(\omega)\frac{\cos\left(\sqrt{k_s^2-k_m^2}z\right)}{\cos\left(\sqrt{k_s^2-k_m^2}L\right)}e^{-ik_m x} + \sum_n \tilde{g}_n(\omega)\frac{\sin\left(\sqrt{k_s^2-k_n^2}(z-L)\right)}{\cos\left(\sqrt{k_s^2-k_n^2}L\right)G\sqrt{k_s^2-k_n^2}}e^{-ik_n x} + \ldots \tag{3.54}$$

The first term is related to the excitation as if it were a free field case. Like we have seen in chapter 2, this term causes the infinite peaks at the natural frequencies. The second term is only related to the stresses at the interface. Both terms go to infinity as $k_s L \to \pi/2 + p\pi$ for $m = n = 0$. $\tilde{f}_0$ is chosen to be positive and $\tilde{g}_0(\omega)$ can be either positive or negative. If $\tilde{g}_0(\omega)$ is positive, both terms add up and the displacement $\tilde{u}_y$ goes to infinity. If $\tilde{g}_0(\omega)$ is negative, both terms cancel each other and the displacement $\tilde{u}_y$ is no longer necessarily infinite. $\tilde{g}_0(\omega)$ can be calculated through equation (3.53) for every frequency ω. As research shows, the sign of $\tilde{g}_0(\omega)$ changes after every natural frequency, causing the alternating pattern of finite and infinite peaks.

Starting at around 46 Hz, we can see another peak “growing” in between other peaks. A third difference with the free field case is that the intervals between peaks are not entirely regular: while the smaller peaks remain at their original frequencies, the large peaks shift towards the left progressively as the frequency increases. This can be seen best in direct comparison to the free field case in figure (3.15).

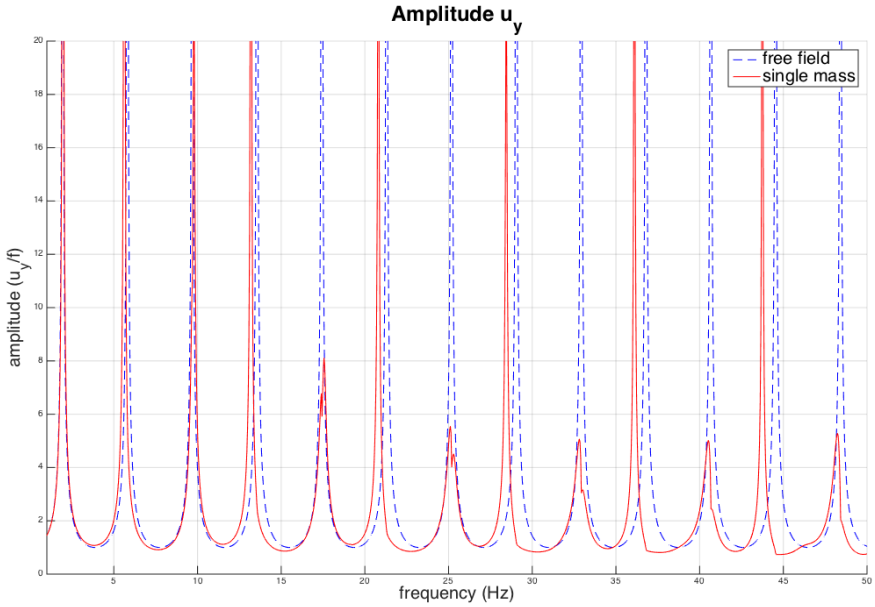

Figure 3.15: transfer function of free field and soil-mass system.

Figure (3.15) shows that the natural frequencies of this system have changed after putting a mass on the top of the soil layer. For some frequencies, the system behaves like a free field system and for other frequencies, the system "senses" that there is a mass on top of the soil layer and the dynamic behaviour is changed. For high frequencies, the interaction stress has more effect on the vibrations of the system than the lower frequencies.

In contrast to the stress distribution at the interface (figure (3.13)), evaluating the transfer function does not require many modes *n* at all. Equation (3.48) shows that only the stress coefficient g_0 plays a role in the equation of motion for the mass, which represents the average stress along the interface. Figure (3.9a), (3.10a) and (3.11a) show that the g_0 is nearly independent of the number of modes used, despite being a fully coupled system of equations. Therefor, considering only $n = 0$ is enough to obtain an accurate transfer function, especially for frequencies below 50 Hz, see figure (3.16), blue line. The range $n = [-1 : 1]$ gives a completely converged result that is indistinguishable from higher orders, see figure (3.16), red line. The red line from figure (3.16) is identical to the line in figure (3.14), which was composed with $n = [-10 : 10]$.

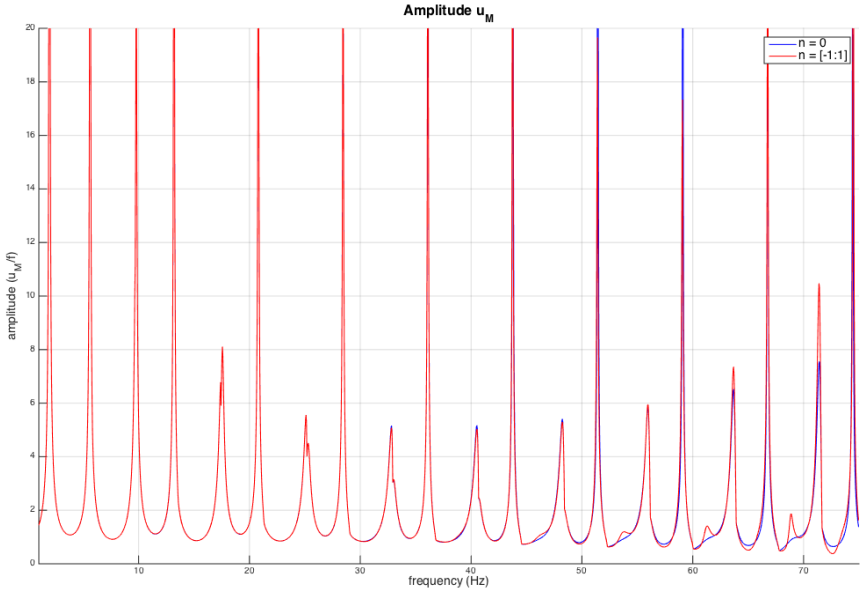

Figure 3.16: transfer function of soil-mass system.

4 Double mass-spring system

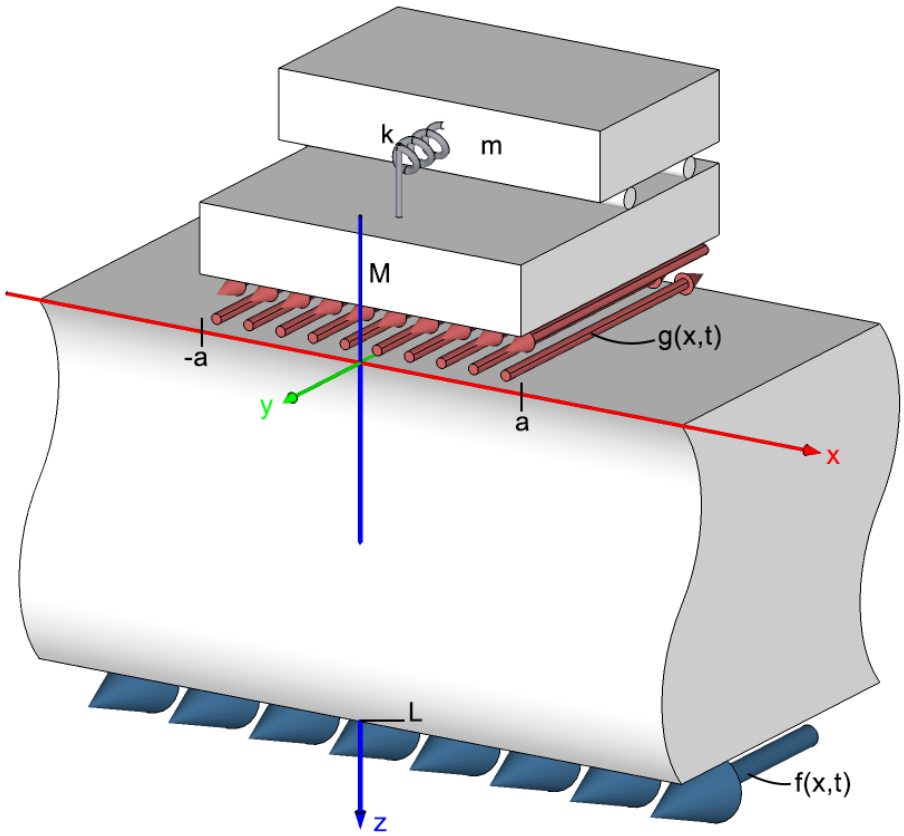

Figure 4.1: a homogeneous elastic soil layer subjected to dynamic, kinematic loading at bottom surface. The red arrows at the top represent the stress function g and the blue arrows at the bottom represent the displacement function f. The structure is modelled as a double mass-spring system.

In this chapter, we will look at the influence that an object consisting of two masses connected by one spring has on the response of the soil at the surface to the excitation at the deep layer. An example of such a structure could be a multi-storey building where the lower mass *M* represents the foundation and the upper mass *m* the rest of the building. Both masses are considered inextensible. The lower mass has the same dimensions as in chapter 2. We assume that the object cannot slip and that the displacement of the lower mass *M* must therefor equal that of the soil. We will look at the shear stresses σ_{zy} between the soil and the foundation again like in chapter 2. Furthermore we are interested in the transfer function of this system compared to free field case and the case of a single mass on the soil. We will also look at the response of the top mass *m* and compare it to a conventional but strongly simplified model.
This chapter follows up on section 3.2 where we derived the solution (3.42) for the equation of motion of the soil. Similar to section 3.3 and 3.4, we follow up by defining new equations of motion for both masses for this specific case and solving the interface condition $\tilde{u}_y = \tilde{u}_M$ at $z = 0$ to obtain a new transfer function.
The double mass-spring system will lead to a coupled set of equations in section 4.1 to describe the motion of both masses. The mass-spring system is subject to the same stress function $g(t, x)$ as defined by equation (3.1) and used in equation (3.46). In section 4.2 we will solve both equations of motion by solving the interface condition between the soil and the foundation mass *M*.

4.1. Equation of motion of mass-spring system

In this section, we derive the equation of motion for the mass-spring system in the time domain and transform it to the frequency domain. We consider two inextensible blocks with masses *M* and *m*, connected by a spring with stiffness *k*. The mass *M* is constrained by the shear stress at the interface with the soil. The equations of motion read

$$M\ddot{u}_M + k(u_M - u_m) = F(t) \tag{4.1}$$

$$m\ddot{u}_m + k(u_m - u_M) = 0 \tag{4.2}$$

Or in matrix notation:

$$\begin{bmatrix} M & 0 \\ 0 & m \end{bmatrix} \begin{bmatrix} \ddot{u}_M \\ \ddot{u}_m \end{bmatrix} + \begin{bmatrix} k & -k \\ -k & k \end{bmatrix} \begin{bmatrix} u_M \\ u_m \end{bmatrix} = \begin{bmatrix} F \\ 0 \end{bmatrix} \tag{4.3}$$

With

M	the mass of the lower block
m	the mass of the upper block
u_M	the displacement of the lower block
u_m	the displacement of the upper block
k	the spring stiffness
F	the external force

Applying the Fourier transform (2.9) to the equations of motion (4.1) and (4.2) yields

$$\tilde{u}_M(k - \omega^2 M) - \tilde{u}_m k = F(\omega) \tag{4.4}$$

$$\tilde{u}_m(k - \omega^2 m) - \tilde{u}_M k = 0 \tag{4.5}$$

Considering that the body is inextensible, we only consider rigid body displacements for the mass. We have seen from equation (3.46) that we can define the force as

$$F(\omega) = \tilde{g}_0(\omega) 2a \tag{4.6}$$

Combining (4.6) with (4.4) and (4.5) gives the explicit equations of motion for the masses in the frequency domain:

$$\tilde{u}_M = -\tilde{g}_0(\omega) \frac{2a(-m\omega^2 + k)}{\omega^2(-Mm\omega^2 + Mk + km)} \tag{4.7}$$

$$\tilde{u}_m = -\tilde{g}_0(\omega) \frac{2ak}{\omega^2(-Mm\omega^2 + Mk + km)} \tag{4.8}$$

Equation (4.7) can be used for the interface condition between the soil and the foundation at the interface surface. From this interface condition, we can derive the coefficients g_n.

4.2. Solving the interface condition

To solve the interface condition at $z = 0$, we combine (3.42) and (4.7) and let $\tilde{u}_y = \tilde{u}_M$. The equation for $\tilde{u}_y$ holds the known excitation modes k_m and coefficients $\tilde{f}_m$ and the unknown stress modes k_n and coefficients $\tilde{g}_n$. The equation for $\tilde{u}_M$ holds the unknown stress modes k_n and coefficients $\tilde{g}_n$. We rearrange the equation such that all unknown terms are on the left hand side and all known excitation terms are on the right hand side:

$$\sum_n \tilde{g}_n(\omega) \frac{\sin\left(\sqrt{k_s^2 - k_n^2}(-L)\right)}{\cos\left(\sqrt{k_s^2 - k_n^2}L\right) G\sqrt{k_s^2 - k_n^2}} e^{-ik_n x}$$

$$+ \sum_n \sum_P \tilde{g}_n(\omega) \frac{\sin\left(|\alpha(P)|(-L)\right)}{\left(\sqrt{k_s^2 - \alpha(P)^2} - k_n\right) GL\sqrt{k_s^2 - \alpha(P)^2}\sin\left(|\alpha(P)|L\right)} e^{ik_n a} e^{-i\sqrt{k_s^2 - \alpha(P)^2}(x+a)}$$

$$+ \sum_n \sum_Q \tilde{g}_n(\omega) \frac{-\sin\left(|\alpha(Q)|(-L)\right)}{\left(-i\sqrt{\alpha(Q)^2 - k_s^2} - k_n\right) GLi\sqrt{\alpha(Q)^2 - k_s^2}\sin\left(|\alpha(Q)|L\right)} e^{ik_n a} e^{-\sqrt{\alpha(Q)^2 - k_s^2}(x+a)}$$

$$+ \sum_n \sum_P \tilde{g}_n(\omega) \frac{-\sin\left(|\alpha(P)|(-L)\right)}{\left(-\sqrt{k_s^2 - \alpha(P)^2} - k_n\right) GL\sqrt{k_s^2 - \alpha(P)^2}\sin\left(|\alpha(P)|L\right)} e^{-ik_n a} e^{i\sqrt{k_s^2 - \alpha(P)^2}(x-a)}$$

$$+ \sum_n \sum_Q \tilde{g}_n(\omega) \frac{\sin\left(|\alpha(Q)|(-L)\right)}{\left(i\sqrt{\alpha(Q)^2 - k_s^2} - k_n\right) GLi\sqrt{\alpha(Q)^2 - k_s^2}\sin\left(|\alpha(Q)|L\right)} e^{-ik_n a} e^{\sqrt{\alpha(Q)^2 - k_s^2}(x-a)}$$

$$+ \tilde{g}_0(\omega) \frac{2a(-m\omega^2 + k)}{\omega^2(-Mm\omega^2 + Mk + km)} = \sum_m \tilde{f}_m(\omega) \frac{-1}{\cos\left(\sqrt{k_s^2 - k_m^2}L\right)} e^{-ik_m x} \tag{4.9}$$

We proceed in a manner analogue to section 3.4. We apply the orthogonality property (equation (3.51)) which leads to a system of coupled equations (3.52). We solve the equations to find the stress coefficients, which are then used to compute the response of the soil to the excitation and compare it to the previous cases.
We will use a numerical approach again and we assume the same parameters as in chapter 3. In addition we assume a value for parameters *m* and *k*. The results from these assumptions are only valid for this specific case and need to be reevaluated when different parameters are used!

Parameters			
ρ	2000 [kg/m³]	M	25 000 [kg]
a	10 [m]	G	3*10⁸ [n/m²]
L	50 [m]	X	10 [m]
k	3*10⁸ [n/m²]	m	25 000 [kg]

Like for the single mass case in chapter 3, the number of poles *p* and the number of modes *n* are to be chosen such that the stress distribution and the transfer function lead to a converged result, based on the assumed parameters. The recommended number of poles remains the same as for the single mass case: for the range $n = [3:3]$, *p* needs a range of roughly $p = [-50:50]$ to converge. For $n = [5:5]$, *p* needs a range of roughly $p = [-100:100]$. For $n = [10:10]$, *p* needs a range of roughly $p = [-150:150]$.

4.2.1. Solving stress coefficients g_n

With equation (3.4) and equation (3.53) we plot the stress coefficients and the distribution at the interface again. Figure (4.2) shows the coefficients $\tilde{g}_n$ and the stress distribution $\tilde{g}(\omega, x)$ for $n = [-3:3]$ at 43.8 Hz and 44.7 Hz. Figure (4.3) shows the coefficients and the stress distribution for $n = [-5:5]$. Figure (4.4) for $n = [-10:10]$.

Figure 4.2a: coefficients g_n, n=[-3:3]

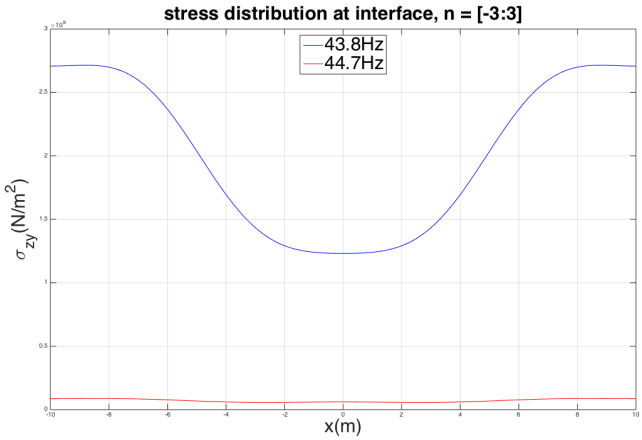

Figure 4.2b: stress distribution, n=[-3:3]

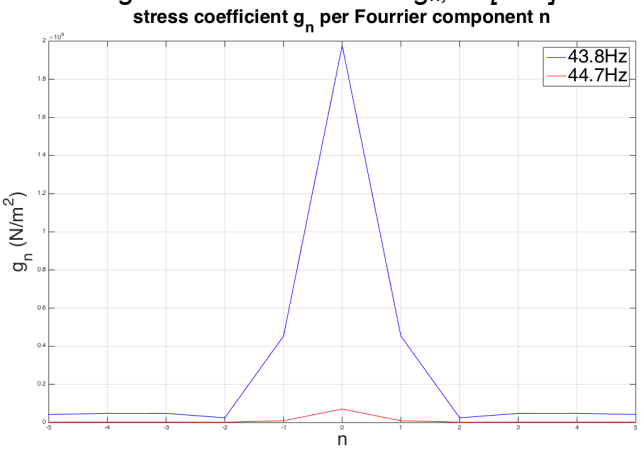

Figure 4.3a: coefficients g_n, n=[-5:5]

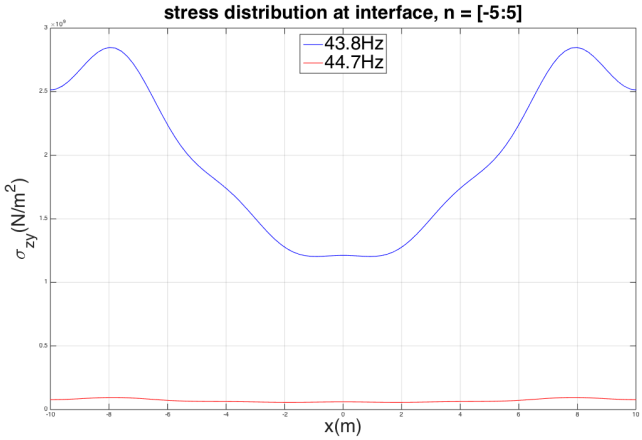

Figure 4.3b: stress distribution, n=[-5:5]

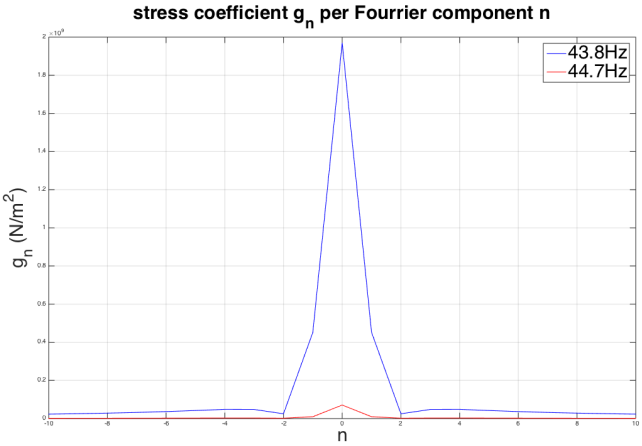

Figure 4.4a: coefficients g_n, n=[-10:10]

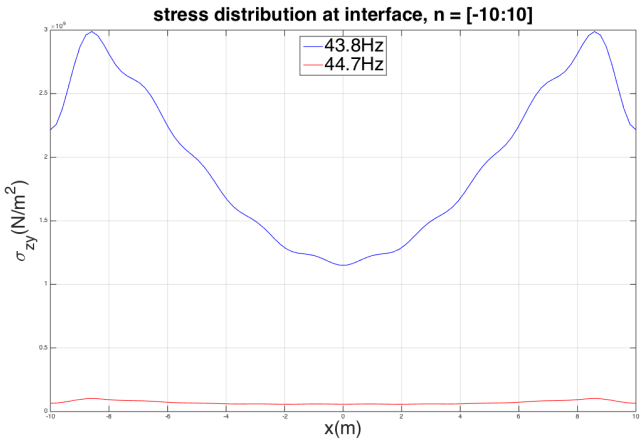

Figure 4.4b: stress distribution, n=[-10:10]

From figure (4.2), (4.3) and (4.4) we can see that the stress coefficients and the stress distribution looks very similar to the single mass case. We see the great relevance of the frequency again where the stresses are much higher for natural frequencies than other frequencies. The frequencies for these examples are also the same as for the single mass case. While the shapes of the coefficient distributions and the stress distributions have the same shape as for the single mass system, the magnitude is about twice as high.

Figure (4.5) shows that the centre part of the stress distribution, roughly in the range of $x = [-6 : 6]$ m, converges quickly and a range for *n* as low as $n = [-3 : 3]$ gives fairly accurate results. At the sides of the interface however, the result has not converged up to $n = [-15 : 15]$ and even more modes are required for accurate results.

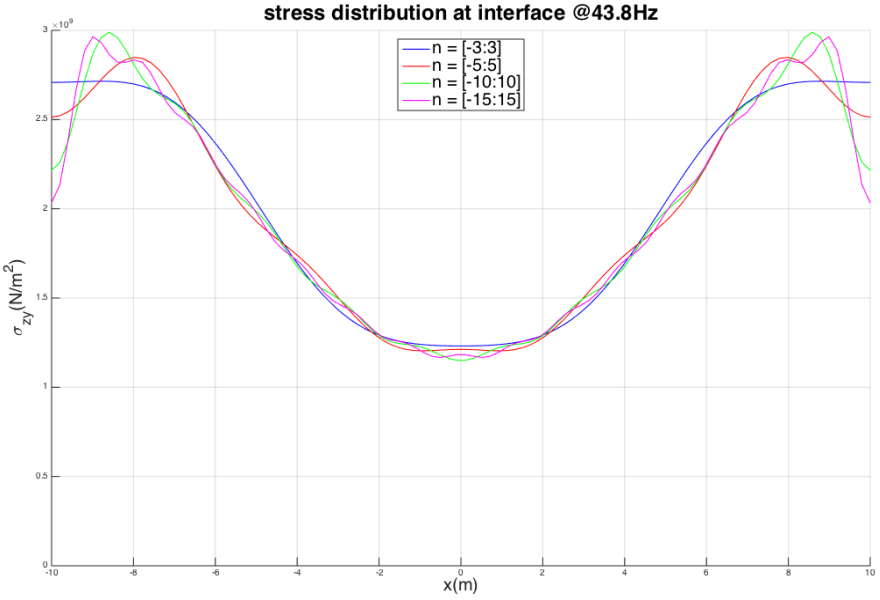

Figure 4.5: stress distribution at interface for different number of modes.

4.2.2. Analysing the transfer function at surface

We now use equation (4.7) to evaluate the displacement of the lower mass $\tilde{u}_M$ and we compare it to the free field case and the single mass case.
The transfer function in figure (4.6) shows a pattern of peaks, indicating the natural frequencies of the system. From approximately 28 Hz upward, we see an alternating pattern of infinitely large peaks and smaller peaks. The reason for this alternating pattern is the same as for the single mass case: the (frequency dependent) coefficient g_0 changes sign after every natural frequency. This means that the first and second term of equation (3.42) either enforce or cancel each other, creating infinite or finite peaks. For frequencies beyond approximately 50 Hz we see another small peak in between the finite and infinite peaks.

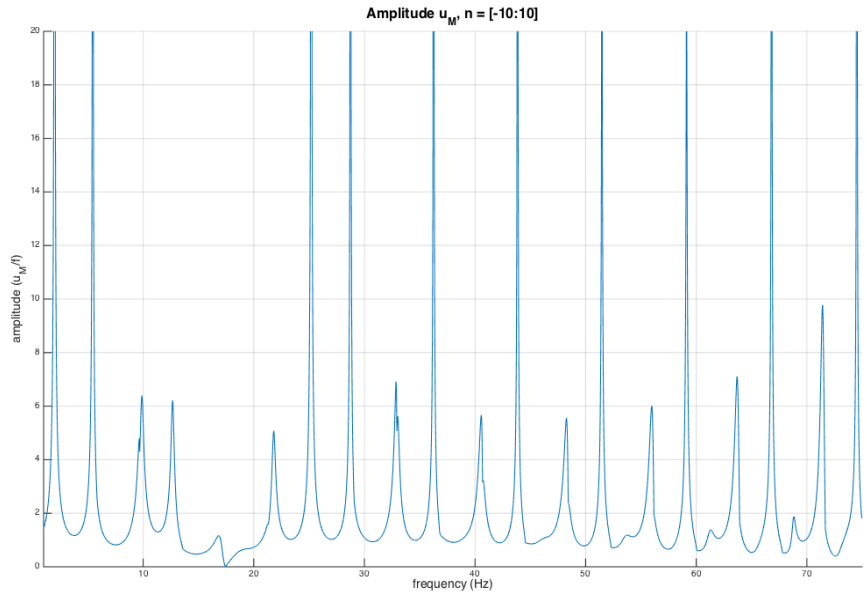

Figure 4.6: transfer function of foundation mass M.

We see a remarkable inconsistency between 10 and 20 Hz were the response is very low and even zero in between. This inconsistency is the result of the added mass-spring system, whose eigenfrequency can be shown to be exactly 17.4 Hz:

$$\omega_n = \sqrt{\frac{k}{m}} = \sqrt{\frac{3 \cdot 10^8}{25000}} = 109.5 \text{ rad/s} = 17.4 \text{ Hz} \tag{4.10}$$

When the system is excited at 17.4 Hz, resonance will occur in the added mass-spring system. As a consequence, all the energy in the system is absorbed by the response of the top mass which stabilises the bottom mass. We will see an increased response when we evaluate the transfer function of the top mass (figure (4.9)).

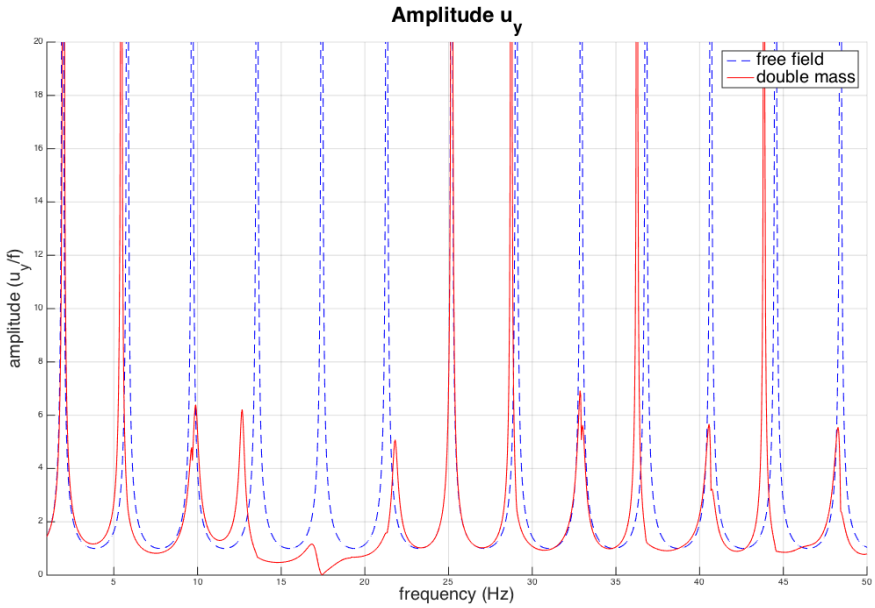

Figure 4.7: transfer function of double mass system compared to free field system.

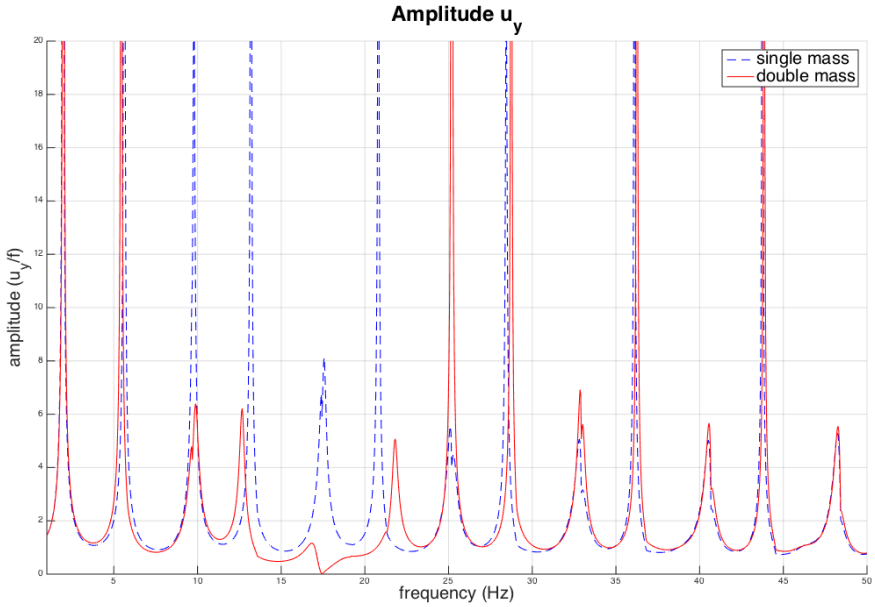

Figure 4.8: transfer function of double mass system compared to single mass system.

In figure (4.7), the transfer function is compared to the free field case. Like for the single mass case (figure (3.15)), we see that the infinite peaks of the double mass system are slightly shifted to the left compared to the free field case. The smaller peaks remain more or less in their place.
In figure (4.8) we compare the transfer function of the double mass-spring system to the single mass system. Aside from the clear differences in the 10 to 25 Hz range, both systems respond very similarly to the excitation, especially the further away you look from the 10 to 25 Hz range.

4.2.3. Analysing the transfer function for the top mass

In figure (4.9) we look at the transfer function for the top mass. We see an equidistant pattern of peaks at the natural frequencies of the system again with alternating heights beyond approximately 50 Hz. These peaks correspond with those we have seen earlier for other transfer functions, as they obviously occur at the same natural frequencies. If you look carefully in the high frequency range, you can see a third peak "growing" in between the regular peaks, similar like we have seen in figure (3.14) and figure (4.6). In the range of 10 to 25 Hz we see an increased response that is related to the eigenfrequency of the mass-spring system at 17.4 Hz. In figure (4.10), the transfer function from figure (4.9) is compared directly with figure (4.6).

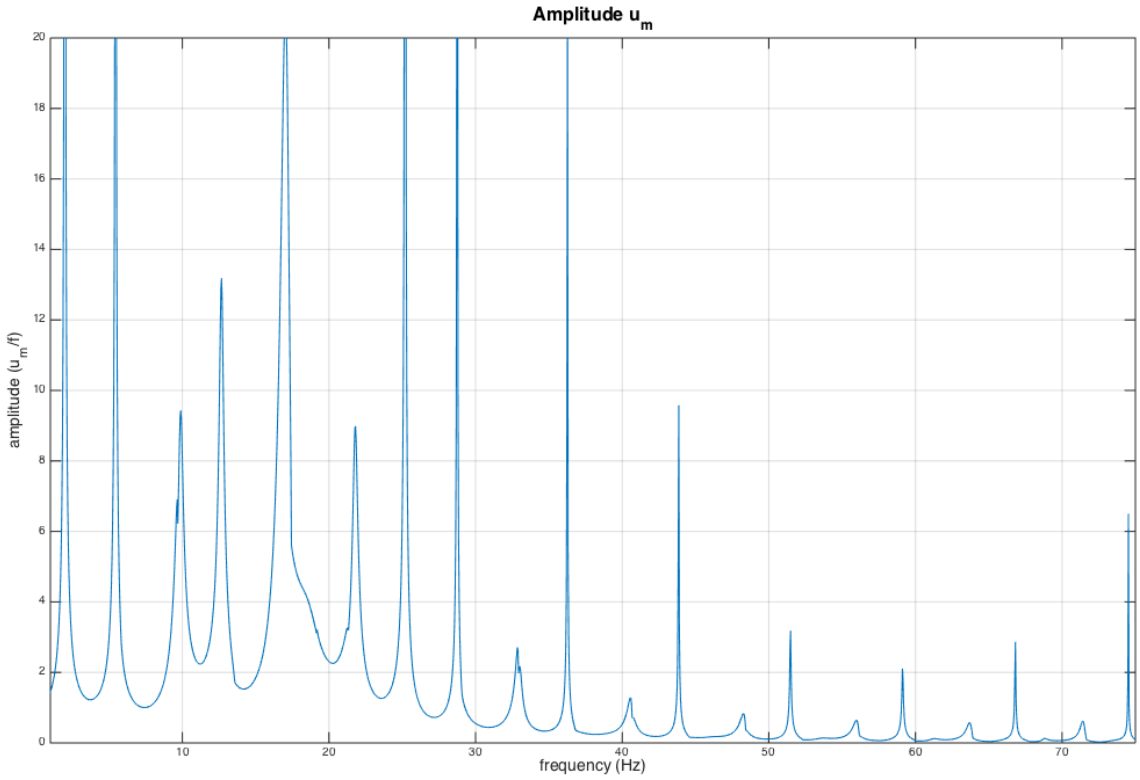

Figure 4.9: transfer function of double mass system compared to single mass system.

To analyse the transfer function of the top mass, we used a completely coupled system: the soil layer, bottom mass and top mass are all coupled and therefor all have an influence on the flexibility matrix of the system. As we have seen, each of these components have a significant influence on the interaction stress and how the system as a whole behaves. We will now touch briefly on an oversimplified model that forms the basis of conventional methods to determine the displacement of the top mass. This oversimplified model does not use a fully coupled system, but analyses the behaviour of the soil layer and the mass-spring system separately. This works in the following way: the soil layer is analysed as a free field case. The transfer function of the soil at the surface is then used as a kinematic excitation of the lower mass, which then excites the top mass-spring system. In essence this means that the interaction stress at the interface between the soil layer and the bottom mass is ignored, which is an extreme oversimplification of reality. We will have brief look at the differences between both models. Let it be clear that this oversimplified model does not do justice to current engineering models in use and should not be viewed as such!

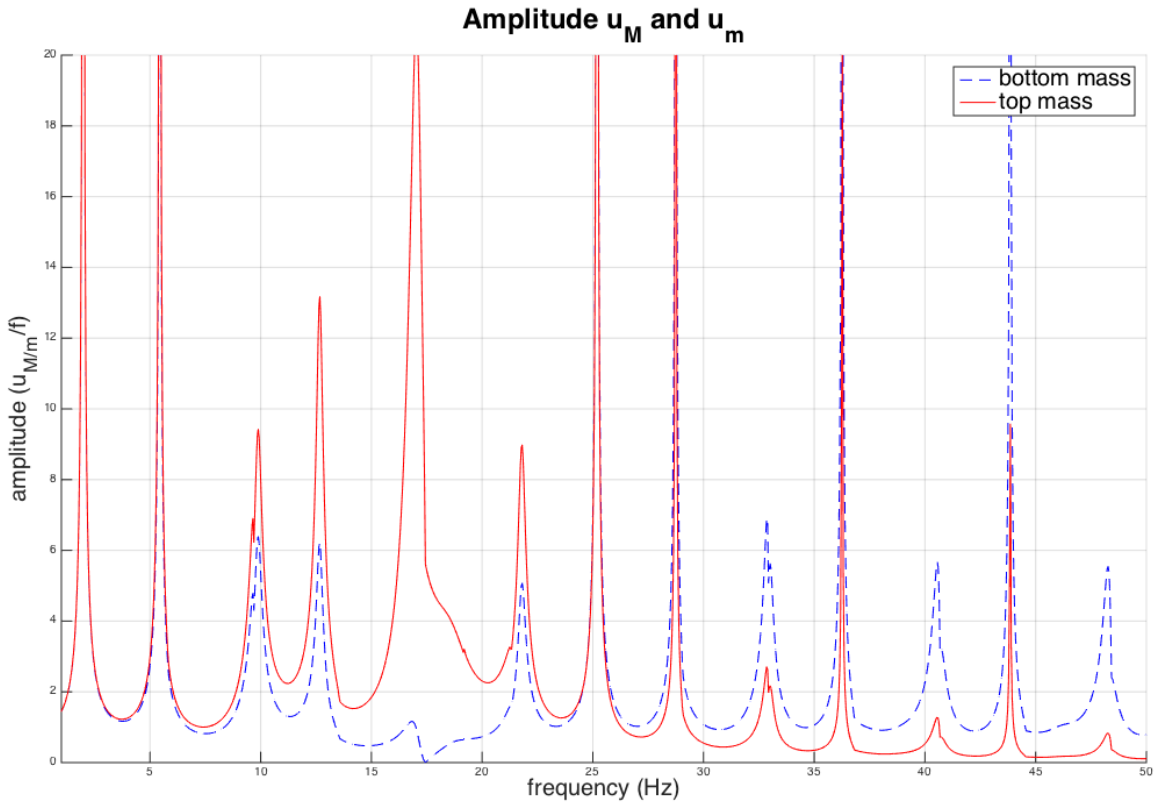

Figure 4.10: transfer function of top mass m compared to bottom mass M.

To relate the response of the top mass, $\tilde{u}_m$, to the kinematic excitation of the bottom mass, $\tilde{u}_M$, we can use equation (4.5):

$$\tilde{u}_m(k - \omega^2 m) - \tilde{u}_M k = 0 \tag{4.11}$$

We can reformulate this to

$$\tilde{u}_m = \tilde{u}_M \frac{1}{1 - \omega^2/\omega_n^2} \tag{4.12}$$

with

$$\omega_n = \sqrt{k/m}$$

If we prescribe the excitation of the bottom mass to be that of the free field surface, we can formulate $\tilde{u}_M$ as

$$\tilde{u}_M = \sum_m \tilde{f}_m(\omega) \frac{1}{\cos\left(\sqrt{k_s^2 - k_m^2} L\right)} e^{-ik_m x} \tag{4.13}$$

In figure (4.11) we compare this “isolated” method to the fully coupled method.

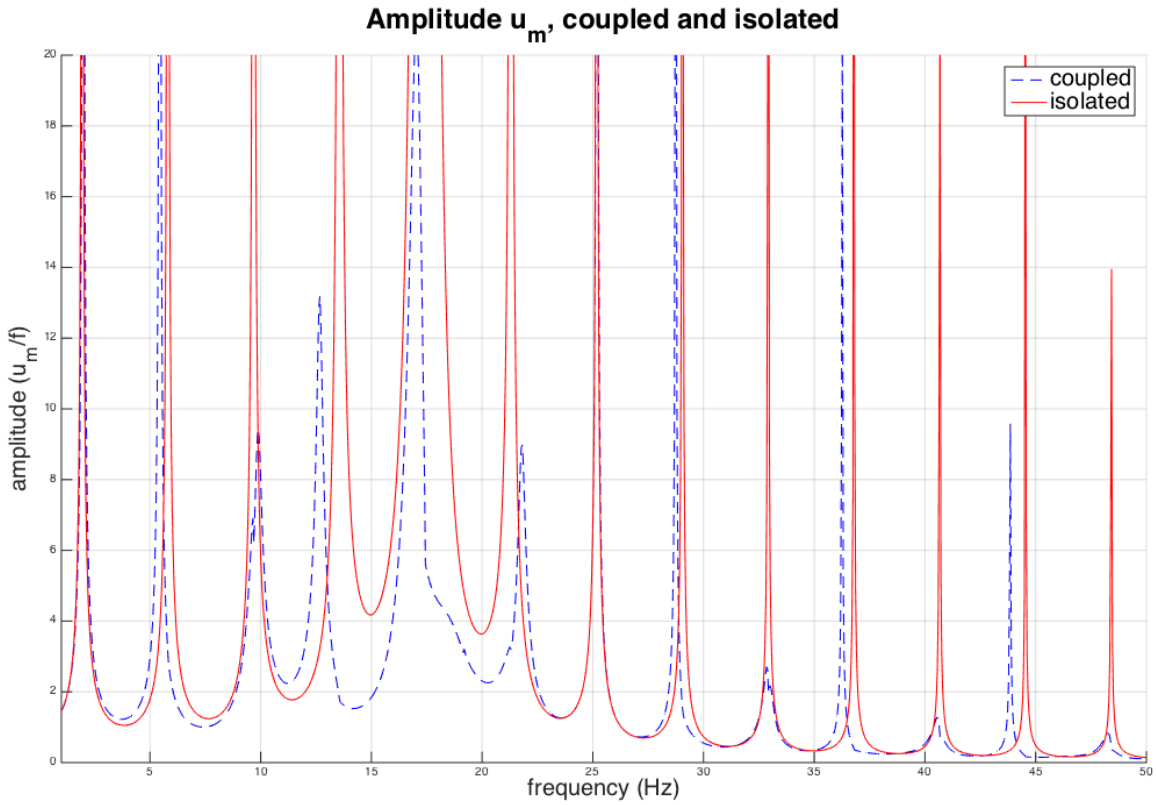

Figure 4.11: transfer function of top mass m, coupled system compared to isolated system.

Figure (4.11) shows that there are significant differences between the isolated and coupled systems. The isolated system shows infinite resonance for all natural frequencies of the soil layer. This is a direct consequence of the fact that the free field response also shows infinite resonance on all natural frequencies. The coupled system shows the alternating pattern on finite and infinite peaks that we have seen in chapter 3 and 4. We also see a shift of the natural frequencies to the left for the coupled system.

The isolated system clearly shows the natural frequency ω_n of the mass-spring system with an increased response. The coupled system also shows this increased response, even though there are clear differences between the two systems.

This comparison shows that the oversimplified model is indeed strongly oversimplified.

5 Conclusion & recommendations

5.1. Conclusion

The goal of this minor thesis is to provide a general framework for calculations for horizontally polarised shear waves in soil with dynamic boundary conditions of displacements and stresses. With this framework, different scenarios can be evaluated where the area, shape and frequency of the excitation and the size and type of the mass-spring system may vary.
The method that was used relies on formulating the specific solution to the equation of motion in terms of Fourier series with unknown coefficients g_n. These coefficients are solved through an interface condition between the soil layer and a mass-spring system that share an interface stress containing coefficients g_n.

The research questions that needed to be answered are:
- How does interaction with objects on the surface impact the behaviour of waves in the soil?
- Will this computational method work?

In chapter 2, we formulated an equation of motion for a soil layer that is excited kinematically at a depth L. By making use of Fourier series, we can allow many different shapes for the excitation. We derived a general solution to the equation of motion and solved it for a free field case. In chapter 3 we solved the general solution for the case that the surface is no longer stress-free. This solution, equation (3.42), forms the general framework that can be applied to various mass-spring systems. We evaluated two of these systems.

The following parameters can easily be adjusted to adapt the governing equation to any specific case:

- excitation shape and frequency, through f_m and k_m
- soil type, through G and ρ
- depth of excitation area, through L
- size, stiffness and mass of the structure, through a, k, M and m

Changing these parameters is straight forward for the most part, with some remarks:

Careful consideration is required when choosing the number of modes for the excitation field. A low number of modes may give an unsatisfactory result when modelling abrupt changes in the excitation shape, like a step function. A high number of modes adds significant computational cost, which in many cases is not desirable. Finding the right balance is key. In the evaluated results, only a uniform displacement is used!

The parameters G, L and ρ will determine the position of the poles on the real and imaginary axis in the complex k_x-plane. These poles have to be selected carefully. Additionally, there are infinitely many poles of type 2 (equation 3.21B) that cannot all be included in the calculation. Therefor, the number of poles p need to be truncated appropriately. How many poles should be included for a reliable result will also depend on the used parameters and cannot be answered a priori.

The stress distribution at the interface highly depends on the excitation frequency and the number of Fourier components used. The latter is especially noticeable at the sides of the interface. Using as many Fourier components as available computational power allows is strongly recommended. On the contrary, when evaluating the transfer functions of the structure, a minimal number of Fourier components will suffice.

5.1.1 impact of interaction stress

The impact of the interaction stress is best visible in figure (3.15) where the transfer function from the single mass case is compared to the free field case. Most noticeable is that the natural frequencies have changed after putting a mass on the top of the soil layer. Resonance occurs at slightly lower frequencies than in the free field case for certain natural frequencies. For other natural frequencies the response seems to be lower

than with a free surface. For high frequencies, the interaction stress has more effect on the vibrations of the system than the lower frequencies.

When evaluating the transfer function of the additional mass-spring system, figure (4.11), it also shows that it is affected by the interaction stress. It also shows an alternating pattern of infinite and finite resonance at the natural frequencies of the system, that are slightly shifted compared to the stress-free interface case. The (resonance) response at the eigenfrequency of the mass-spring system is less regular compared to the oversimplified, isolated case.

5.1.2 Will this computational method work?

Yes. We tested the computational method, where we use generalised boundary conditions on the soil layer and mass system that are then solved through an interface condition, on two specific cases and the outcome meets all expectations. The transfer functions show an expected pattern of resonance peaks that show a lot of resemblance to the free field case, that was solved in a conventional method. This shows a degree of the reliability of the outcome. The transfer function of the double mass-spring system also shows the eigenfrequency of the mass-spring system through a high excitation of the top mass and a much lower excitation of the bottom mass at 17.4 Hz. It clearly shows that this computational method can also handle more complex, multi degree of freedom systems. The coupled systems also show differences when compared to the free field case and the isolated mass-spring system, like shifting of the natural frequencies and the amplitude of the response. These differences underline the relevance of taking interaction stresses into account.

5.2. Recommendations

The scenario that was considered in this study is limited by a very strict scope. Some assumptions were made that only reflect a part of reality and therefor it is important to consider a few things when using the results of this study in practice.

The scope of this study is limited to horizontally polarised shear waves. It is rather unlikely for this scenario to happen and therefor the results of this study should always be used in combination with other wave types like vertically polarised shear waves, longitudinal waves and surface waves.

So far we have only considered a 2D model and we assumed the gradient in y-direction to be zero. This is not always a realistic model and therefor an expansion in 3D should be considered for a more realistic model.

We only considered a homogeneous, infinite soil layer. In reality, you may find multiple soil layers with different characteristics and other boundaries in the soil. Evaluating an inhomogeneous elastic continuum might be of interest for further study.

When we evaluated the transfer function of the top mass in chapter 4, we compared it to an oversimplified, isolated model. While this isolated model is the basis of more conventional methods, it does no justice to current standards. This isolated model could be improved by applying additional springs and dashpots at the soil-structure interface. Doing so would give a fairer comparison to see the real benefits of a fully coupled system.

Bibliography

Hölscher, P. (2016). *Soil Dynamics in urban areas*. Lecture notes CIE5340, Delft University of Technology, Delft.

Metrikine A.V. *Dynamics, Slender Structures and an Introduction to Continuum Mechanics*. Lecture notes CIE4145, Delft University of Technology, Delft.

Saff, E. B., & Snider, A. D. (2003). *Fundamentals of Complex Analysis with Applications to Engineering, Science, and Mathematics* (3rd ed.). Upper Saddle River, USA: Pearson Education, Inc..

Spijkers J.M.J., Vrouwenvelder A.W.C.M., Klaver E.C. (2005). *Structural Dynamics Part 1 - Structural Vibrations*, Lecture notes CIE4140, Delft University of Technology, Delft.

Van Dalen, K. N. (2006). *Ground vibrations induced by a high-speed train running over inhomogeneous subsoil.* Delft University of Technology, Delft.

Van Dalen K. N. (2015). *Soil Dynamics, part B: Body waves in an elastic continuum & Rayleigh waves at the free surface*. Lecture notes CIE5340, Delft University of Technology, Delft.

Appendix A Equation of motion of an elastic continuum

This appendix gives a derivation for a set of equations of motion in a homogeneous elastic continuum which are used to describe the dynamic behaviour of the continuum.

A.1. General

A cartesian axis-system is used in three dimensions. The coordinate system is called the *x*-*y*-*z*-system. The displacement is described by three components: u_x, u_y and u_z in *x*, *y*, and *z* direction respectively. These components are degrees of freedom of a particle and in general these quantities vary in time and in space.
This appendix uses the index notation together with the application of the summation convention. The index notation uses the notation σ_{ij} where *i* and *j* are *x*, *y*, *z* in a 3D space. The first index gives the direction of the outward normal of the surface, the second index gives the direction in which the force works. The summation convention means that identical indices are summed over all space dimensions.
A stress is considered positive if the external force works in the same direction as the external normal of the surface, i.e. tension. If the external force works opposite to the direction of the external normal, i.e. compression, the stress is considered negative. Stresses with identical indices are normal stresses, stresses with non-identical indices are shear stresses.

Derivatives
In soil dynamics, variables depend on time and space and the first and second derivative with respect to these quantities play an important role. A short notation can be used to avoid complex writing, that is in agreement with the index notation and makes a distinction between partial derivates for space coordinates and time.
A partial derivative with respect to space is written in the subscript index, separated by a comma. A time derivative is shown by a single super- imposed dot, the second time derivative by a double super-imposed dot:

$$\frac{\partial u_x}{\partial x} = u_{x,x} \qquad \frac{\partial u_x}{\partial y} = u_{x,y} \qquad \frac{\partial u_i}{\partial t} = \dot{u}_i \qquad \frac{\partial^2 u_i}{\partial t^2} = \ddot{u}_i$$

A.2. Governing equations

To derive the equations of motion for the homogeneous elastic continuum, kinematic, constitutive and equilibrium equations need to be combined.

A.2.1. Kinematic equations

The kinematic equations relate the displacements to the strains. For the shear strain, it holds that

$$\varepsilon_{ij} = \frac{1}{2}\left(\frac{\partial u_i}{\partial j} + \frac{\partial u_j}{\partial i}\right) = \frac{1}{2}\left(u_{i,j} + u_{j,i}\right) \tag{A.1}$$

For the shear deformation, the relation between the shear angle and the strain must be derived. The angle between two originally perpendicular lines changes by γ. From geometry, we find that the angle can be approximated by

$$\frac{1}{2}\gamma = \frac{\partial u_y}{\partial x} = \frac{\partial u_x}{\partial y} \tag{A.2}$$

Summation of these two equations results in

$$\gamma = \frac{\partial u_y}{\partial x} + \frac{\partial u_x}{\partial y} = 2\varepsilon_{ij} \tag{A.3}$$

This equation relates the angle of deformation and the strain in the material.

A.2.2. Constitutive equations

The constitutive equations relate the stresses to the strains. In a continuum, two types of deformations are possible:

- An isotropic deformation where the volume of the material changes, but angles between lines do not change.
- A shear deformation where the volume of the material does not change, but the angles between lines do.

For the isotropic deformation, the relation between the isotropic stress and the volumetric strain is

$$\sigma_0 = K\varepsilon_{vol} \tag{A.4}$$

$$\sigma_0 = \frac{1}{3}\sigma_{ii} = \frac{1}{3}(\sigma_{xx} + \sigma_{yy} + \sigma_{zz}) \tag{A.5}$$

$$\varepsilon_{vol} = \varepsilon_{ii} = \varepsilon_{xx} + \varepsilon_{yy} + \varepsilon_{zz} \tag{A.6}$$

with

K	the bulk modulus [Pa]
σ_0	the isotropic stress [Pa]
σ_{ii}	the normal stress component in the *i* direction [Pa]
ε_{vol}	the volumetric strain
ε_{ii}	the strain component in the *i* direction

For the shear deformation, the relation between the shear stress and the angle of deformation is

$$\tau = G\gamma \tag{A.7}$$

For the shear stress, it holds that

$$\tau = \sigma_{ij} = \sigma_{ji} \tag{A.8}$$

Together with equation (A.3), it follows that

$$\sigma_{ij} = 2G\varepsilon_{ij} \tag{A.9}$$

A.2.3. Equilibrium equations

For the equilibrium equations, Newton's second law applies: the sum of all forces in direction *i* gives the mass an acceleration in direction *i*, which is the second time derivative of the displacement. The contributing forces include the change in normal stresses and shear stresses, multiplied by their respective surface. For an infinitesimal cube, this results in the following equilibrium equations:

$$\begin{aligned}
\frac{\partial \sigma_{xx}}{\partial x} + \frac{\partial \sigma_{yx}}{\partial y} + \frac{\partial \sigma_{zx}}{\partial z} &= \rho \frac{\partial^2 u_x}{\partial t^2} \\
\frac{\partial \sigma_{xy}}{\partial x} + \frac{\partial \sigma_{yy}}{\partial y} + \frac{\partial \sigma_{zy}}{\partial z} &= \rho \frac{\partial^2 u_y}{\partial t^2} \\
\frac{\partial \sigma_{xz}}{\partial x} + \frac{\partial \sigma_{yz}}{\partial y} + \frac{\partial \sigma_{zz}}{\partial z} &= \rho \frac{\partial^2 u_z}{\partial t^2}
\end{aligned} \tag{A.10}$$

In full index notation:

$$\sigma_{ij,j} = \rho \ddot{u}_i \tag{A.11}$$

A.3. Generalisation of Hooke's law

For a bar, unconstraint in lateral directions, the following linear relation known as Hooke's law holds:

$$\sigma_{xx} = E \varepsilon_{xx} \tag{A.12}$$

with

x	the coordinate along the axis of the bar [Pa]
E	the Young's modules [Pa]
σ_{xx}	the normal stress in the bar [Pa]
ε_{xx}	the strain in the bar

While the lateral stresses (σ_{yy} and σ_{zz}) are zero, the lateral strains (ε_{yy} and ε_{zz}) are not. Based on the linearity of the load and the strain, the lateral strains are proportional to the load and thus the strain ε_{xx}:

$$\varepsilon_{yy} = \varepsilon_{zz} = -\nu \varepsilon_{xx} \tag{A.13}$$

where ν is the lateral contraction coefficient or "Poisson's ratio".
This leads to Hooke's law for a continuum in three dimensions. In vector notation:

$$\begin{bmatrix} \varepsilon_{xx} \\ \varepsilon_{yy} \\ \varepsilon_{zz} \end{bmatrix} = \begin{bmatrix} 1/E & -\nu/E & -\nu/E \\ -\nu/E & 1/E & -\nu/E \\ -\nu/E & -\nu/E & 1/E \end{bmatrix} \begin{bmatrix} \sigma_{xx} \\ \sigma_{yy} \\ \sigma_{zz} \end{bmatrix} \tag{A.14}$$

Inverting this equation leads to

$$\begin{bmatrix} \sigma_{xx} \\ \sigma_{yy} \\ \sigma_{zz} \end{bmatrix} = \frac{E}{(1+\nu)(1-2\nu)} \begin{bmatrix} 1-\nu & \nu & \nu \\ \nu & 1-\nu & \nu \\ \nu & \nu & 1-\nu \end{bmatrix} \begin{bmatrix} \varepsilon_{xx} \\ \varepsilon_{yy} \\ \varepsilon_{zz} \end{bmatrix} \tag{A.15}$$

A.4. Summary of constitutive equations

Relation (A.15) can be simplified by using the geotechnical useful bulk modulus *K* and shear modulus *G:*

$$K = \frac{E}{3(1-2\nu)} \qquad G = \frac{E}{2(1+\nu)} \tag{A.16}$$

Recalling the relation between the shear stress and shear strain from (A.9) we can compliment (A.15) to the full constitutive equation for the linear elastic continuum. In vector notation:

$$\begin{bmatrix}\sigma_{xx}\\ \sigma_{yy}\\ \sigma_{zz}\\ \sigma_{xy}\\ \sigma_{yz}\\ \sigma_{zx}\end{bmatrix} = \begin{bmatrix} K+\frac{4}{3}G & K-\frac{2}{3}G & K-\frac{2}{3}G & 0 & 0 & 0\\ K-\frac{2}{3}G & K+\frac{4}{3}G & K-\frac{2}{3}G & 0 & 0 & 0\\ K-\frac{2}{3}G & K-\frac{2}{3}G & K+\frac{4}{3}G & 0 & 0 & 0\\ 0 & 0 & 0 & 2G & 0 & 0\\ 0 & 0 & 0 & 0 & 2G & 0\\ 0 & 0 & 0 & 0 & 0 & 2G \end{bmatrix} \begin{bmatrix}\varepsilon_{xx}\\ \varepsilon_{yy}\\ \varepsilon_{zz}\\ \varepsilon_{xy}\\ \varepsilon_{yz}\\ \varepsilon_{zx}\end{bmatrix} \tag{A.17}$$

In index notation:

$$\sigma_{ij} = \left(K - \frac{2}{3}G\right)\varepsilon_{kk}\delta_{ij} + 2G\varepsilon_{ij} \tag{A.18}$$

Where δ_{ij} is the Kronecker δ defined by

$$\delta_{ij} = \begin{cases} 1 & \text{if } i = j \\ 0 & \text{if } i \neq j \end{cases} \tag{A.19}$$

A.5. Equation of motion

Having found the kinematic, constitutive and equilibrium equations, the equation of motion can be derived. Recalling from (A.1) that

$$\varepsilon_{ij} = \frac{1}{2}(u_{i,j} + u_{j,i}) \tag{A.20}$$

We conclude that

$$\varepsilon_{kk} = u_{k,k} \tag{A.21}$$

Substituting (A.21) in the constitutive equation (A.18) leads to

$$\sigma_{ij} = \left(K - \frac{2}{3}G\right)u_{k,k}\delta_{ij} + G\left(u_{i,j} + u_{j,i}\right) \tag{A.22}$$

Substituting (A.22) in the equilibrium equation (A.11) requires differentiation with respect to space:

$$\sigma_{ij,j} = \left(K - \frac{2}{3}G\right)u_{k,kj}\delta_{ij} + G\left(u_{i,jj} + u_{j,ij}\right) \tag{A.23}$$

The summation convention also applies to derivate indices, which leads to the fact that differentiation and summation are included in one single step. This gives us the equation of motion for an elastic continuum:

$$\left(K - \frac{2}{3}G\right)u_{k,ki} + G\left(u_{i,jj} + u_{j,ij}\right) = \rho\ddot{u}_i \tag{A.24}$$

Appendix B Contour integration and Cauchy's residue theorem

This appendix summarises a method from the field of complex analysis to evaluate complex integrals. This method includes contours in the complex plane, poles and the residue theorem. This method is used in section 2.3 to evaluate the inverse Fourier transform of the equation of motion.

B.1. Poles and residues

When a function $f(z)$ is defined on the complex *z*-plane and a singularity occurs at $z = a$, the function cannot be expanded in a Taylor series around $z = a$. Instead, it can be expanded in a *Laurent* series of the form

$$f(z) = \frac{b_p}{(z-a)^p} + \frac{b_{p-1}}{(z-a)^{p-1}} + \ldots + \frac{b_1}{(z-a)} + a_0 + a_1(z-a) + \ldots \tag{B.1}$$

Or

$$f(z) = \sum_{n=1}^{p} b_p (z-a)^{-p} + \sum_{n=0}^{\infty} a_n (z-a)^n \tag{B.2}$$

If $f(z)$ is analytical on $0 < |z-a| < r$, where *r* is the distance to the nearest singularity and of the form of (B.1), then *a* is said to be a *pole* of order *p*. A pole of order one is also called a *simple pole*.

In general, we can say that *a* is a pole of order *p* for $f(z)$ if

$$\lim_{z \to a} (z-a)^p f(z) \tag{B.3}$$

exists and is not zero.

The coefficient of $(z-a)^{-1}$ is called the *residue* of $f(z)$ at the pole $z = a$. The residue of a function is important when evaluating complex integrals. To find the residue of $f(z)$ at the simple pole $z = a$, we consider a general case:

$$f(z) = \frac{b_1}{(z-a)} + a_0 + a_1(z-a) + \ldots \tag{B.4}$$
$$(z-a)f(z) = b_1 + a_0(z-a) + a_1(z-a)^2 + \ldots$$

From this, we conclude that

$$\operatorname*{Res}_{z=a} f(z) = b_1 = \lim_{z \to a} (z-a) f(z) \tag{B.5}$$

If $f(z)$ has a pole of order *p* at $z = a$, the residue of $f(z)$ at $z = a$ can be found as

$$\operatorname*{Res}_{z=a} f(z) = b_1 = \frac{1}{(p-1)!} \lim_{z \to a} \frac{d^{p-1}}{dz^{p-1}} \left[(z-a)^p f(z) \right] \tag{B.6}$$

B.2. Cauchy's residue theorem

Consider a regular function $f(z)$ in the complex *z*-plane and a closed contour *C* like in figure (B.1).

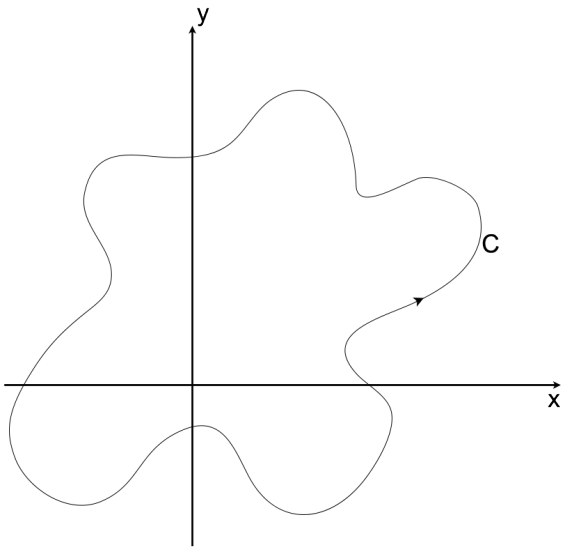

Figure B.1: Closed curve in complex z-plane.

Cauchy's theorem states that if $f(z)$ is regular within and on a closed contour *C*, then

$$\oint_C f(z)dz = 0 \tag{B.7}$$

If the function $f(z)$ is not regular at a finite number of poles within the contour *C*, we need to adapt the contour to make it regular inside again. To do so, we "cut out" the pole $z = a$ by drawing a small circle *Γ* around it with centre $z = a$ and radius *r* in opposite direction of *C*. We connect *Γ* to *C* with a cut *AB*, see figure (B.2). Now inside and on the closed curve defined by *C*, *AB*, *Γ* and *BA*, the function $f(z)$ is regular again.

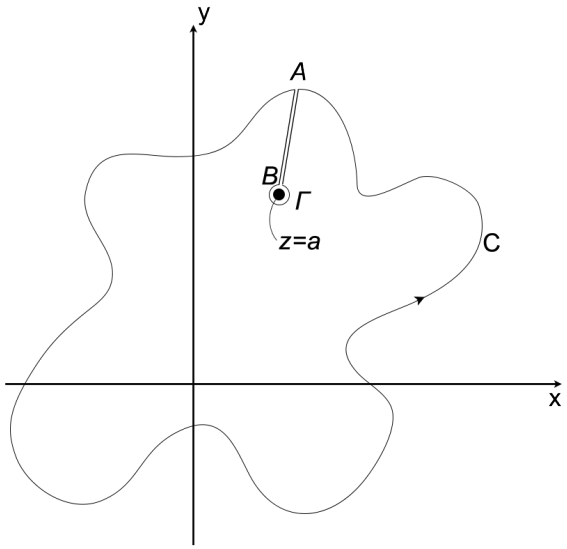

Figure B.2: Closed curve in complex z-plane with a pole.

From (B.7) we then find

$$\oint_C f(z)dz + \int_{AB} f(z)dz + \oint_\Gamma f(z)dz + \int_{BA} f(z)dz = 0 \tag{B.8}$$

The integrals over AB and BA cancel out as the are the same integral in opposite direction, hence:

$$\oint_C f(z)dz = -\oint_\Gamma f(z)dz = \oint_{-\Gamma} f(z)dz \tag{B.9}$$

The sign of *-Γ* indicates that the integral is taken in the opposite direction, which is the same direction as for *C*. On *-Γ*, *z* can be written as

$$z = a + re^{i\theta} \tag{B.10}$$

To evaluate the integral over *-Γ*, it holds that

$$\int_\Gamma f(z)dz = \int_a^b f\left(\Gamma(\theta)\right)\frac{d\Gamma(\theta)}{d\theta}d\theta \tag{B.11}$$

We combine (B.10), (B.11) and (B.2) and let $0 \leqslant \theta \leqslant 2\pi$. We can then write the integral around *-Γ* as

$$\begin{aligned}\oint_{-\Gamma} f(z)dz &= \int_0^{2\pi}\left[\sum_{n=1}^{p}\frac{b_n}{r^n e^{in\theta}} + \sum_{n=0}^{\infty} a_n r^n e^{in\theta}\right] ire^{i\theta}d\theta \\ &= ir\int_0^{2\pi}\left[\sum_{n=1}^{p}\frac{b_n}{r^n}e^{i(1-n)\theta} + \sum_{n=0}^{\infty} a_n r^n e^{i(n+1)\theta}\right] d\theta\end{aligned} \tag{B.12}$$

The integral of (B.12) has the form of

$$\int_0^{2\pi} e^{iN\theta}d\theta = \left[\frac{e^{iN\theta}}{iN}\right]_0^{2\pi} = \begin{cases} 2\pi & \text{if } N = 0 \\ 0 & \text{if } N \neq 0 \end{cases} \tag{B.13}$$

Hence, we conclude that

$$\oint_C f(z)dz = \oint_{-\Gamma} f(z)dz = 2\pi i b_1 = 2\pi i \operatorname*{Res}_{z=a}\left(f(z)\right) \tag{B.14}$$

When there are multiple poles within C, we can repeat the process above for each pole and sum up their results. This leads us to what is called the residue theorem:

$$\oint_C f(z)dz = 2\pi i \sum_n \operatorname*{Res}_{z=z_n}\left(f(z)\right) \tag{B.15}$$

Note that the integral has to be taken counter clockwise along C. If the integral is taken clockwise, the right hand side of (B.15) will have a minus sign.

Contour integration together with the residue theorem is a very powerful method to evaluate complex integrals.